Energy & Environmental Science

REVIEW

View Article Online
View Journal | View Issue

Cite this: *Energy Environ. Sci.*, 2020, **13**, 24

Conjugated polymers for visible-light-driven photocatalysis

Chunhui Dai and Bin Liu *

Received 18th June 2019,
Accepted 30th September 2019

DOI: 10.1039/c9ee01935a

rsc.li/ees

Conjugated polymers have recently been under active investigation as promising alternatives to traditional inorganic semiconductors for photocatalysis. This is due to their unique advantages of low cost, high chemical stability, and molecularly tunable optoelectronic properties. This critical review summarizes the recent advancements in π-conjugated polymers for visible-light-driven photocatalytic applications including water splitting, CO_2 reduction, organic transformation and degradation of organic dyes. Special emphasis is placed on how the changes in the polymer structure could influence their physicochemical properties and photocatalytic activities. This structure–activity relationship analysis should guide rational molecular design of conjugated polymers for improved photocatalytic activity.

Broader context

The exploitation of efficient photocatalysts to directly convert the radiant sunlight into chemical energy is of great importance to address the current energy and environmental challenges. Conjugated polymers (CPs) consisting of photoactive π-systems represent an attractive platform for solar energy utilization. They have been intensively studied for a variety of photocatalytic applications and many exciting performances were reported through facile molecular design. A comprehensive review is thus timely to summarize the progress of the field. This review article systematically presents the recent advances in conjugated polymers for visible-light-driven photocatalysis, including water splitting, CO_2 reduction, organic transformation and degradation of organic dyes. The synthesis and design principles of conjugated polymers in these photocatalytic applications are illustrated, with an emphasis on the correlation between polymer structures and their photocatalytic activities. We expect that the systematic discussion in this review will not only provide a general overview of the field, but also promote the development of conjugated polymers with fascinating properties for photocatalysis.

1. Introduction

The sun is known as a super "energy warehouse" to irradiate solar light continuously to the Earth. On average, the solar energy reaching the Earth's surface per hour is enough to meet

Department of Chemical & Biomolecular Engineering, National University of Singapore, 117585, Singapore. E-mail: cheliub@nus.edu.sg

Chunhui Dai

Chunhui Dai obtained his PhD degree (2016) in organic chemistry from the School of Chemistry and Chemical Engineering at Nanjing University, China. He is now a Research Fellow in Prof. Bin Liu's research group at the Department of Chemical and Biomolecular Engineering, National University of Singapore. His research interest is centred on the design and synthesis of conjugated polymers for photocatalytic conversions.

Bin Liu

Bin Liu is currently Provost's Chair Professor in the Department of Chemical and Biomolecular Engineering at the National University of Singapore (NUS), where she received her PhD degree in 2001. After postdoctoral work at the University of California, Santa Barbara, she joined NUS in late 2005. Her research focuses on the development of conjugated polymers and organic nanomaterials and exploration of their applications in sensing, imaging and solar energy conversion.

the current human energy demand in a whole year.[1,2] Despite the advantages of inexpensive, abundant and clean features of sunlight, it is difficult to utilize solar energy very efficiently because of its low energy density as well as diffuse and intermittent nature. Therefore, it is desirable to convert sunlight into chemical energy, which represents an appealing solution to address several challenges facing the world today. For example, clean hydrogen fuel production by photocatalytic water splitting holds great promise to alleviate the global energy crisis, which promises to be clean, renewable and eco-friendly.[3–9] Enabling photocatalytic technology will also allow the reduction of CO_2 into value-added chemicals (CO, CH_4, and CH_3OH, *etc.*), thereby creating huge benefits by simultaneously solving the current energy shortage and environmental issues caused by overloaded CO_2 release.[10–14] Moreover, light-driven organocatalysis is considered as an attractive strategy for direct chemical bond functionalization with a broad substrate scope under mild conditions, which is a vitally important contribution to organic synthetic methodology.[15–20] Last but not least, photocatalytic degradation of organic dyes in wastewater is a powerful technology for environmental remediation.[21–24]

In a photocatalytic process, the photon energy required for photoexcitation is dependent on the optical gap of the photocatalyst. As compared to the UV region that comprises only 5% of solar light, the visible light (400–800 nm) accounts for about 53% of the incident solar energy (Fig. 1).[4,25,26] Therefore, it is crucial to develop photocatalysts with optical gap below 3.0 eV to increase the absorption of solar light with a focus on the visible light region.

Over the past few decades, research efforts have been intensively devoted to pursuing suitable photocatalysts for practical applications. Among them, organic π-conjugated polymers have recently garnered significant attention as promising candidates for various photocatalytic applications. Many interesting features allow π-conjugated polymers to stand out in the field of photocatalysis over inorganic semiconductors. Firstly, they are environmentally friendly semiconductor materials, consisting of earth-abundant elements, and they possess tunable energy levels for oxidation and reduction reactions. Secondly, they could be facilely prepared under mild conditions and have excellent chemical stability against photobleaching. Thirdly, their molecular structures can be fine-tuned to better utilize visible light, while many traditional inorganic photocatalysts are only UV-active. Last but not least, the π-conjugation along the polymer backbone enables them with unique photogenerated charge carrier separation and transport properties, which is critical to trigger photoredox reactions.

Upon diverse modification of conjugated polymers (CPs) at the molecular level, many exciting achievements in photocatalysis have recently been reported, which clearly justify a comprehensive review on this research topic. So far, most CP based photocatalysis reviews have been based on the family of graphitic carbon nitride (g-C_3N_4) materials with a focus on one or two photocatalytic applications.[18,27–35] There is an urgent need to provide a review focused on π-conjugated polymers in photocatalysis from a broad perspective to present an overview of the recent developments on this research topic.

This review presents the recent advances of CPs in applications of photocatalytic water splitting, CO_2 photoreduction, light-driven organic transformation and photocatalytic degradation of organic dyes (Fig. 2). We focus on an in-depth understanding of how the CP structure modification could influence the optical properties, photogenerated charge separation and transport, and photocatalytic activity. The review starts from a brief discussion of general photocatalytic processes and the synthesis of CP photocatalysts. This is followed by the illustration of CPs for each photocatalytic application. Finally, perspectives toward exploring new CPs for photocatalytic applications are proposed, which is expected to stimulate the future development of more exciting CPs for photocatalysis.

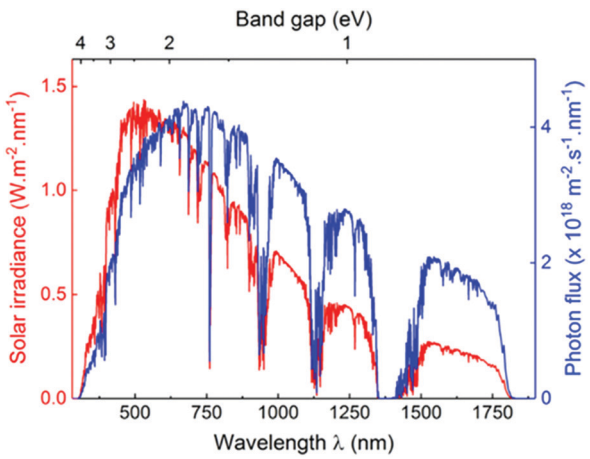

Fig. 1 AM1.5 solar light radiation spectrum (red) and photon flux curve (blue) as functions of light wavelength and material band gap. Reprinted with permission from ref. 25. Copyright 2017 Wiley-VCH.

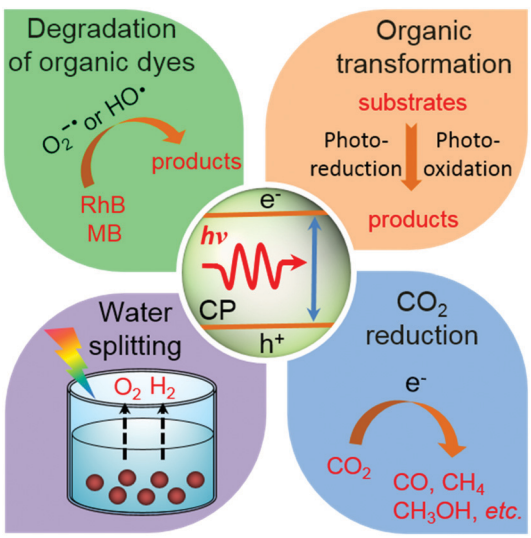

Fig. 2 Overview of π-conjugated polymers for various photocatalytic applications, which are summarized in this review.

2. Basic aspects of π-conjugated polymers for photocatalytic applications

2.1 Fundamentals of heterogeneous photocatalysis

The main processes of polymeric semiconductors in specific light-driven redox reactions are described in many reviews[3,11,14,27,28,36–39] and the general pathway is briefly illustrated in Fig. 3a. Upon light irradiation, the semiconductor harvests incident photons and charges (electron–hole pairs) are formed inside the photocatalyst. The photogenerated charges subsequently separate and migrate to the semiconductor surface where redox reactions take place. On the other hand, most of the photogenerated electrons and holes could undergo bulk or surface recombination, which are competitive processes to the surface reactions.

According to the proposed mechanism of photocatalytic redox reactions, an efficient CP photocatalyst should at least have the following properties: (a) a strong and broad absorption in the visible region to effectively capture solar light; (b) high charge separation and migration efficiency for surface redox reactions; (c) appropriate energy level alignments to enable efficient charge separation as well as the reduction or oxidation half reaction. Therefore, light harvesting, energy levels as well as photogenerated charge separation and migration are three key factors affecting the photocatalytic activities of these CPs (Fig. 3b). This requires rational design and synthesis of CPs for effective photocatalysis.

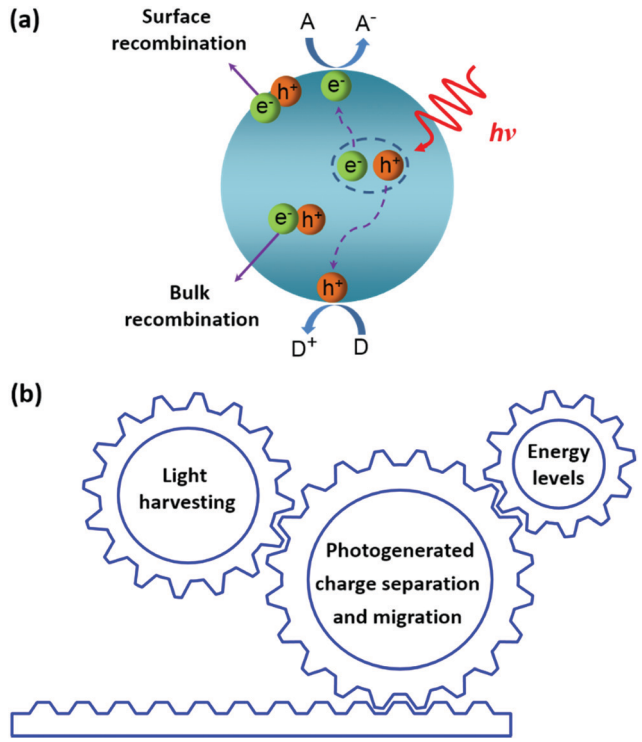

Fig. 3 (a) The main process of polymeric semiconductors for photocatalysis (D: electron donor; A: electron acceptor) and (b) critical factors affecting their photocatalytic performances.

2.2 Synthesis of conjugated polymers for heterogeneous photocatalysis

The extensively available conjugated organic monomers and diverse synthetic methods enable facile synthesis of a broad range of CPs. Moreover, the polymer structures could be precisely controlled for specific photocatalytic applications. Among these methods, Pd-catalyzed Suzuki–Miyaura coupling polymerization between halogenated aromatics and diboronyl ester has been widely used to prepare linear copolymers and conjugated porous polymers (Fig. 4). The reaction is typically carried out in the presence of a base (always K_2CO_3) under a N_2 or Ar atmosphere. Another commonly used method for preparing CPs by C–C coupling is the Sonogashira coupling reactions of aromatic halides and terminal alkynes, in which $Pd(PPh_3)_2Cl_2$ was employed as the catalyst with an amine as the base, and CuI as the cocatalyst. Furthermore, Ni(0)-promoted Yamamoto dehalogenation coupling reaction is a convenient pathway to synthesize CPs from dibromo-aromatic monomers. In this reaction, $Ni(COD)_2$ and 2,2′-bipyridyl are used as the catalyst and promoter for polymerization, respectively. Oxidative coupling reactions are exploited as a versatile methodology for performing self-polymerization of arylethynylene monomers, in which CuBr is used as the catalyst and a base is used as the binding agent.

Interestingly, conjugated polymer nanomaterials could be readily prepared under appropriate reaction conditions. For example, conjugated microporous polymer nanosheets could be obtained by one-step oxidative coupling of aromatic alkynes[40] or a condensation reaction.[41,42] Conjugated microporous polymer nanoparticles could be directly prepared by polymerization in high internal phase emulsion, which is concentrated emulsion with a dispersed phase volume fraction over 74.05%.[43,44] The morphologies of nanoparticles can be varied by introducing monomers with different electron-donating/withdrawing properties.[45]

Additionally, the condensation reaction between amino and aldehyde groups based on Schiff-chemistry is widely performed to prepare crystalline covalent organic frameworks (COFs) for photocatalysis.[51] The reaction is typically performed under harsh experimental conditions with carefully controlled temperature (usually 120 °C), pressure and reaction time (usually 3–5 days). Acetic acid is employed as the catalyst in the reaction. It is believed that an error-correction process occurs during the conversion of amorphous intermediates to crystalline products. The reaction solvent is crucial for the assembly of framework units. In a typical condensation reaction, mesytilene/dioxane and *n*-butanol/*o*-dichlorobenzene are commonly used reaction solvents. Besides, a suitable building block is also important to obtain a highly crystalline COF. Rigid and planar π-conjugated units are preferred to prepare 2D COFs.

Covalent triazine frameworks (CTFs) could be prepared by a trimerization reaction of aromatic nitriles in the presence of a Brønsted or Lewis acid catalyst.[53] In a typical ionothermal preparation, $ZnCl_2$ is chosen as the catalyst and high temperature (>400 °C) is always required for the reversible reaction. By contrast, a much lower temperature (<100 °C) could be employed

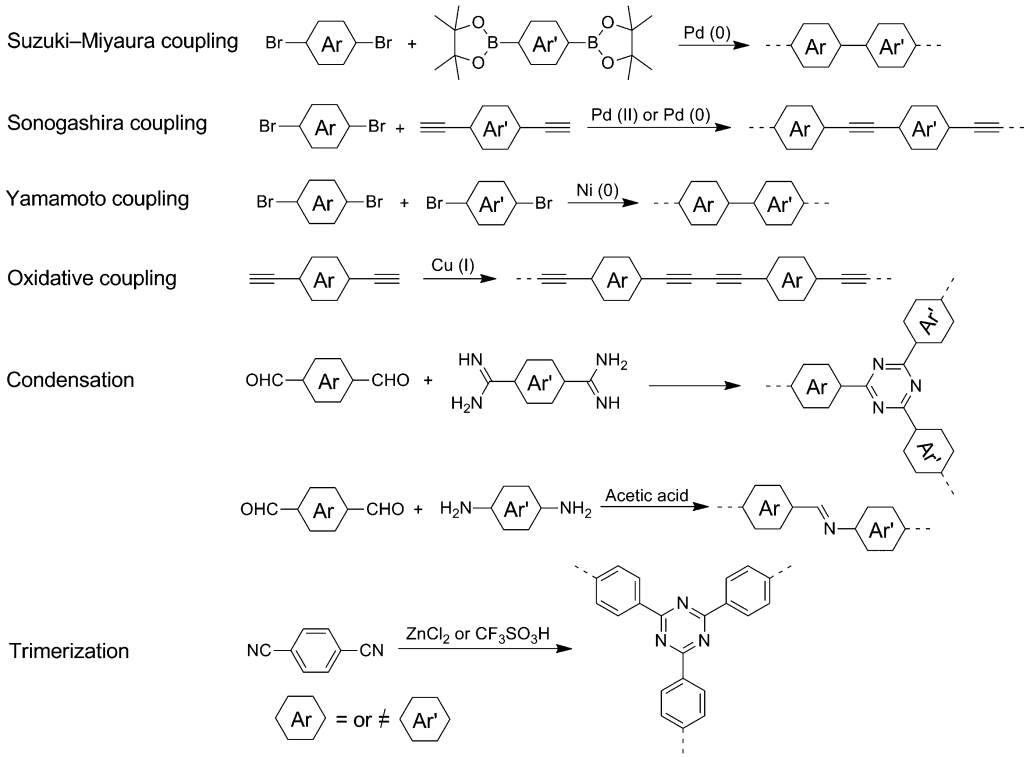

Fig. 4 Typical polymerization methods used to synthesize conjugated polymers for photocatalysis.

when CF_3SO_3H is used as the catalyst for the condensation reaction. Alternatively, CTFs could be synthesized by condensation of an aldehyde and an amidine dihydrochloride, which involves the generation of a Schiff base followed by Michael addition. The reaction is carried out in DMSO with Cs_2CO_3 as a base.

Graphitic carbon nitride (g-C_3N_4) consisting of *s*-triazine or tri-*s*-triazine (heptazine) units has been synthesized by thermal polycondensation of nitrogen-rich precursors, such as melamine, thiourea, urea, dicyanadiamide and cyanamide, *etc.*[18,29,31] For more detailed preparation of the above-mentioned CPs, please refer to other reviews[46–53] and books.[54,55]

3. Conjugated polymers for photocatalytic water splitting

Photocatalytic water splitting is of particular interest as the technology provides an effective pathway for clean hydrogen production using water and sunlight, both of which are abundant in nature.

In a light-driven water splitting process, photogenerated electrons and holes were used for the reduction and oxidation of water, respectively. The photocatalytic reaction is a thermodynamically uphill reaction and a Gibbs free energy (ΔG_0) of +237.2 kJ mol^{-1} is required.[3] In principle, to drive the redox half reaction, the energy level alignments of the polymer photocatalyst and the redox potential of water must be well matched. This means that the lowest unoccupied molecular orbital (LUMO) of the polymer photocatalyst should be more negative than the reduction potential of H^+/H_2 (0 eV *vs.* normal hydrogen electrode (NHE), pH = 0), while its highest occupied molecular orbital (HOMO) must be more positive than the oxidation potential of O_2/H_2O (1.23 eV *vs.* NHE, pH = 0). Therefore, the band gap (E_g) of the polymer should be over 1.23 eV to trigger water splitting. In this part, we summarize the state-of-the-art advancements in photocatalytic H_2 evolution using various types of organic CPs, and their applications in photocatalytic O_2 evolution and overall water splitting are also briefly described.

3.1 Photocatalytic H_2 evolution

Hydrogen is an ideal fuel with gravimetric energy density up to 142 MJ kg^{-1}, which is almost three times larger than that of gasoline.[56] More importantly, H_2 combustion produces water with no pollution to the environment. Photocatalytic hydrogen evolution using semiconductors is a sustainable and economical technology to convert solar energy into hydrogen energy. Since Honda and Fujishima reported water splitting on TiO_2 photoelectrodes in 1972, a huge number of semiconductors have been studied for hydrogen production.[3,34,57–64]

As promising photocatalysts, CPs have been employed for hydrogen production in the early 1980s. Unfortunately, they haven't attracted much attention until three-dimensional (3D) poly(azomethine) networks were demonstrated to be efficient photocatalysts for hydrogen production from water in 2010.[65] Since then, various types of organic CPs have been developed to yield greatly improved H_2-production efficiency. This was achieved through the optimization of CP photophysical properties,

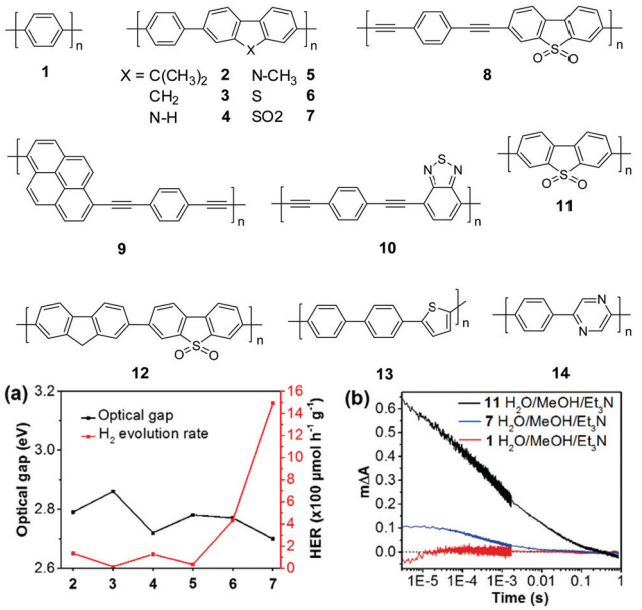

Fig. 5 Chemical structures of polymers **1–14**, (a) the correlation between the photocatalytic H_2 evolution and their optical gaps of polymers **2–7** (>420 nm); (b) transient kinetics probed at 630 nm for polymers **1**, **7**, and **11** in the $Et_3N/CH_3OH/H_2O$ mixture (excited at 355 nm). Reprinted with permission from ref. 72. Copyright 2018 Nature Publishing Group.

mainly light harvesting in the visible region, band gap alignment, as well as photogenerated charge generation and transport, *etc.*

3.1.1 Linear conjugated polymers. The early report of linear organic CPs as the photocatalyst for water splitting could be dated back to 1985.[66] Yanagida *et al.* prepared poly(*p*-phenylene) (PPP) (**1**, Fig. 5) by the polycondensation of 1,4-dibromobenzene. Polymer **1** shows a band gap of 2.9 eV and a hydrogen evolution rate (HER) of 207.5 μmol h^{-1} g^{-1} under broad spectrum irradiation (>290 nm). However, this polymer is almost inactive under visible light (>400 nm). Following this work, they further reported some analogues of 1, but very low activities were achieved even with the assistance of Ru nanoparticles.[67–69]

In 2016, Cooper and co-workers demonstrated the new breakthrough in H_2 evolution by incorporating extended planarized units into the main chain of **1**, which is expected to facilitate the photogenerated charge dissociation and thus promote the proton reduction reaction.[70] Polymers **2–7** show band gaps ranging from 2.70 to 2.86 eV (Fig. 5a). Among them, polymers **2** and **4** exhibited an almost equal HER of ~128 μmol h^{-1} g^{-1}, which was 3-fold improvement over **1**. More excitingly, polymer **7** with the lowest band gap of 2.70 eV exhibited an impressive HER of 1492 μmol h^{-1} g^{-1}, which was 46-fold higher than that of 1 (Table 1).

Encouraged by the good activity of polymer 7, Chen *et al.* further modified this polymer by introducing an ethynyl group into the main chain, which led to a reduced band gap and accelerated charge separation of the resulting polymers. Polymer **8** has a band gap of 1.89 eV and showed a HER of up to 6023 μmol h^{-1} g^{-1} when triethanolamine (TEOA) was used as the sacrificial agent (>420 nm).[71] Similarly, compared to their counterparts without ethynyl insertion, polymers **9** and **10** showed large red shifts of 167 and 154 nm in their light absorption edges, respectively. The HER was enhanced to 4270 μmol h^{-1} g^{-1} for **9** and 3187 μmol h^{-1} g^{-1} for **10**.

Notably, dibenzo[*b*,*d*]thiophene sulfone has been recognized as one of the most attractive building blocks for the synthesis of H_2-production polymer photocatalysts. As shown above, many polymers with incorporated sulfone units show outstanding photocatalytic performances. To study the critical role of the sulfone unit in H_2 evolution, Cooper and co-workers investigated the photophysical properties of polymers **1**, **7** and **11**.[72] Compared with **1** and **7**, the homopolymer of sulfone **11** showed a much higher HER of 3260 μmol h^{-1} g^{-1}. The decay kinetics at 630 nm exhibited a significantly larger signal for **11** than **7**, while almost no signal was observed for **1** (Fig. 5b). This result indicated a higher polaron concentration of **11** and **7**, which is in line with the H_2 evolution activities of the three polymers. Recently, they further prepared nanoparticles of about 160 nm using polymer **11** by mini-emulsion polymerization.[73] With a polymer concentration of 0.1 mg mL^{-1}, the nanoparticle suspension yielded a HER of 14.52 mmol h^{-1} g^{-1}, while a significantly lower HER of 6.13 mmol h^{-1} g^{-1} was measured for the bulk material of **11**, evidently suggesting a size-dependent H_2 evolution of the polymer. Moreover, when the polymer concentration was deceased to 13 μg mL^{-1}, the suspension gave a superior average HER of 60.6 mmol h^{-1} g^{-1} over 5 h, which is the highest value among the reported organic polymers so far.

To further extend the conjugation degree of polymer **7**, we introduced large planar units (fluorene and pyrene) into the main chain.[74] Polymer **12** exhibited a smaller band gap of 2.07 eV in comparison with 7 (2.70 eV) and a good HER of 5040 μmol h^{-1} g^{-1} was achieved. Very recently, Wang *et al.* reported an analogue of polymer **12** by replacing the fluorene in the main chain with electron-rich dibenzothiophene to construct a local D–A heterojunction, which led to a reduced exciton binding energy from **91** to **88** meV and 1.3-fold HER as compared to **12** in the presence of TEOA.[75]

Another modification of PPP (**1**) is the copolymerization of 2,5-phenylene with heterocycles, which results in optimized band gaps and energy levels of the as-prepared polymers. A maximum HER enhancement of 6.5-fold compared to PPP was achieved by polymer **13** with 33% thiophene fraction and a band gap of 2.42 eV.[76] Polymer **14** bearing a 2,5-pyrazine attained a 15-fold higher HER than PPP.[77]

Compared to those insoluble bulk polymers, the development of soluble CPs provides a good choice for easy processing of polymers into a desirable pattern for photocatalytic H_2 production. By virtue of its inherent hydrophobicity, CP could be self-assembled into polymer dots (Pdots) in water.[78–80] Pdots have much smaller size relative to the bulk materials; hence, the distance covered by photogenerated charges migrating to the surface of photocatalyst particles becomes short, and the recombination probability of electrons and holes decreases to improve the photocatalytic efficiency.[81] In 2016, Tian *et al.* prepared a Pdot suspension by the nano-precipitation method using polymer **15** and a matrix polymer PS–PEG–COOH.[82] In the preparation, the mixture of polymer and matrix in THF

Table 1 Summary of representative photocatalytic H_2 evolution using CPs under visible light

Polymer	Optical gap (eV)	S_{BET} ($m^2\ g^{-1}$)	Cocatalyst	Sacrificial agent	Light source[a]	HER ($\mu mol\ h^{-1}\ g^{-1}$)	AQY[b] (%)	Ref.
1	2.9	—	—	DEA	>400 nm (Xe)	Trace	—	66
2	2.79	—	—	TEA	>420 nm (Xe)	136	—	70
3	2.86	—	—	TEA	>420 nm (Xe)	16	—	70
4	2.72	—	—	TEA	>420 nm (Xe)	128	—	70
5	2.78	—	—	TEA	>420 nm (Xe)	36	—	70
6	2.77	—	—	TEA	>420 nm (Xe)	432	1.1	70
7	2.70	—	—	TEA	>420 nm (Xe)	1492	2.3	70
8	1.89	—	—	TEOA	>420 nm (Xe)	6023	4.2	71
9	1.64	—	—	TEOA	>420 nm (Xe)	4270	0.85	71
10	1.94	—	—	TEOA	>420 nm (Xe)	3187	—	71
11	2.62	—	—	TEA	>420 nm (Xe)	3260	11.6	72
12	2.07	—	—	TEA	>420 nm (Xe)	5040	2.13	74
13	2.42	17	—	TEA	>420 nm (Xe)	420	—	76
14	2.45	69	—	TEA	>420 nm (Xe)	960	—	77
15	2.38	—	—	AA	>420 nm (LED)	8300	~0.73	82
16	1.98	—	—	AA	>420 nm (LED)	50 000	~0.88	83
17	2.46	—	—	AA	>420 nm (LED)	NA	—	83
18	2.03	—	—	DEA	>420 nm (LED)	12 700	—	84
19	2.11	—	—	TEA	>420 nm (Xe)	512	—	89
20	—	—	Pt	AA	>420 nm (Xe)	12 800	0.13	90
21	2.33	995	—	DEA	>420 nm (Xe)	174	—	96
22a	1.81	39	—	TEA	>400 nm (Xe)	17	—	105
22b	1.95	59	—	TEA	>400 nm (Xe)	140	—	105
23a	2.89	228	—	TEA	>400 nm (Xe)	397	—	105
23b	2.45	279	—	TEA	>400 nm (Xe)	1460	—	105
24a	2.31	121	—	TEA	>400 nm (Xe)	260	—	105
24b	2.19	99	—	TEA	>400 nm (Xe)	786	—	105
25a	2.33	80	—	TEA	>400 nm (Xe)	414	—	105
25b	2.06	104	—	TEA	>400 nm (Xe)	1900	—	105
26	1.88	—	—	TEA	>400 nm (Xe)	2590	—	106
27	2.44	280	Pt	TEOA	>420 nm (Xe)	400	—	107
28	2.18	58	—	TEOA	≥420 nm (Xe)	9600	1.8	110
29	2.19	499	Pt	TEOA	>420 nm (Xe)	30	—	111
30	2.21	669	Pt	TEOA	>420 nm (Xe)	134	—	112
31	2.28	750	Pt	TEOA	>420 nm (Xe)	598	—	112
32	2.14	564	Pt	TEOA	>420 nm (Xe)	908	2.0	112
33	2.37	834	Pt	TEOA	>420 nm (Xe)	620	—	112
34	2.53	811	—	TEOA	>420 nm (Xe)	2460	—	113
35	2.62	915	—	TEOA	>420 nm (Xe)	188	—	113
36	2.64	447	—	TEOA	>420 nm (Xe)	116	—	113
37	2.84	895	—	TEA	>420 nm (Xe)	120	—	114
38	2.56	431	—	TEA	>420 nm (Xe)	3106	13.2	115
39	2.37	723	—	TEOA	>420 nm (Xe)	5697	—	116
40	2.11	692.5	Pt	TEOA	>420 nm (Xe)	2103.2	6.4	117
41	2.8	1603	Pt	TEOA	>420 nm (Xe)	1970	—	119
42	2.67	702	Pt	TEOA	420–900 nm (Xe)	22.5	—	120
43	2.68	326	Pt	TEOA	420–900 nm (Xe)	90	0.08	120
44	2.62	1537	Pt	TEOA	420–900 nm (Xe)	438	0.19	120
45	2.65	1046	Pt	TEOA	420–900 nm (Xe)	1703	0.44	120
46	2.10	985	Pt	AA	>420 nm (Xe)	4440	—	121
47	1.85	1288	Pt	AA	>420 nm (Xe)	10 100	—	121
48	2.28	919	Pt	AA	>420 nm (Xe)	1600	—	121
49	2.34	523	Pt	TEOA	≥395 nm (Xe)	30	—	122
50	2.31	758	Pt	TEOA	≥395 nm (Xe)	324	1.8	122
51	2.09	541	Pt	TEOA	>420 nm (Xe)	8300	—	123
52	2.06	348	Pt	TEOA	>420 nm (Xe)	1560	—	123
53	1.92	162	Pt	TEOA	>420 nm (Xe)	220	—	123
54	2.03	602	Pt	TEOA	>420 nm (Xe)	1360	—	124
55	2.94	19	Pt	TEOA	≥420 nm (Xe)	200	—	128
56	2.38	52	Pt	TEOA	>420 nm (Xe)	6600	7.3	130
57	2.22	807	Pt	TEOA	>420 nm (Xe)	1238	—	132
58	2.13	764	Pt	TEOA	>420 nm (Xe)	1582	—	132
59	2.33	663	Pt	TEOA	>420 nm (Xe)	1460	—	132
60	2.42	757	Pt	TEOA	>420 nm (Xe)	2647	—	132
61	2.17	569	Pt	TEOA	>420 nm (Xe)	10 760	4.07	133
62	2.47	533	Pt	TEOA	>420 nm (Xe)	5320	4.11	133
63	2.67	650	Pt	TEOA	>420 nm (Xe)	1440	2.10	133
64	—	599	Pt	TEOA	>420 nm (Xe)	5100	—	138
65	—	520	Pt	TEOA	>420 nm (Xe)	2400	—	138
66	—	598	Pt	TEOA	>420 nm (Xe)	650	—	138

Table 1 (*continued*)

Polymer	Optical gap (eV)	S_{BET} (m^2 g^{-1})	Cocatalyst	Sacrificial agent	Light source[a]	HER (μmol h^{-1} g^{-1})	AQY[b] (%)	Ref.
CN–F	2.63	—	Pt	TEOA	>420 nm (Xe)	~130	—	142
CN–N	2.65	9.21	Pt	TEOA	>400 nm (Xe)	553.5	—	143
CN–C/P	2.98	141.1	Pt	TEOA	>420 nm (Xe)	1493.3	2.14	144
CN–BA	2.57	22	Pt	TEOA	>420 nm (Xe)	294	—	145
CN–P15	—	—	—	TEOA	>420 nm (Xe)	722.3	—	152
CN–P17	2.24	—	—	TEOA	>400 nm (Xe)	929.3	5.7	153
CN–PyP	2.46	120	—	TEOA	≥420 nm (Xe)	600	—	154
CN–COF	—	85.2	Pt	TEOA	>420 nm (Xe)	10 100	—	155
CN–CTF	—	—	Pt	TEOA	≥420 nm (Xe)	850	—	156

[a] Xe: xenon lamp. [b] At 420 nm. NA: no activity; AQY: apparent quantum yield; HER: hydrogen evolution rate; DEA: diethylamine; TEA: trimethylamine; TEOA: triethanolamine; AA: ascorbic acid.

was injected into pure water under sonication, and a clear Pdot suspension was obtained after THF evaporation (Fig. 6). The as-prepared Pdots displayed an impressive initial rate of 8300 μmol h^{-1} g^{-1}. Compared to polymer **15**, Pdots of polymer **16** with extended absorption renders an excellent initial HER of up to 50 mmol h^{-1} g^{-1}.[83] The theoretical calculations suggested that N atoms in the 2,1,3-benzothiadiazole (BT) units provided the reactive sites in the formation of hydrogen, polymer **17** without a BT unit did not show any activity although its optical gap and reduction potential are appropriate for proton reduction. Using the nano-precipitation method, Chou *et al.* prepared cycloplatinated Pdots using polymer **18**, which provided an impressive HER of 12.7 mmol h^{-1} g^{-1}, while only 1.3 and 5.46 mmol h^{-1} g^{-1} were obtained for Pdots without a Pt complex and their Pt-complex-blended counterpart under identical conditions, respectively.[84] This was likely attributed to the improved charge transfer after grafting the Pt complex into the polymer backbone.

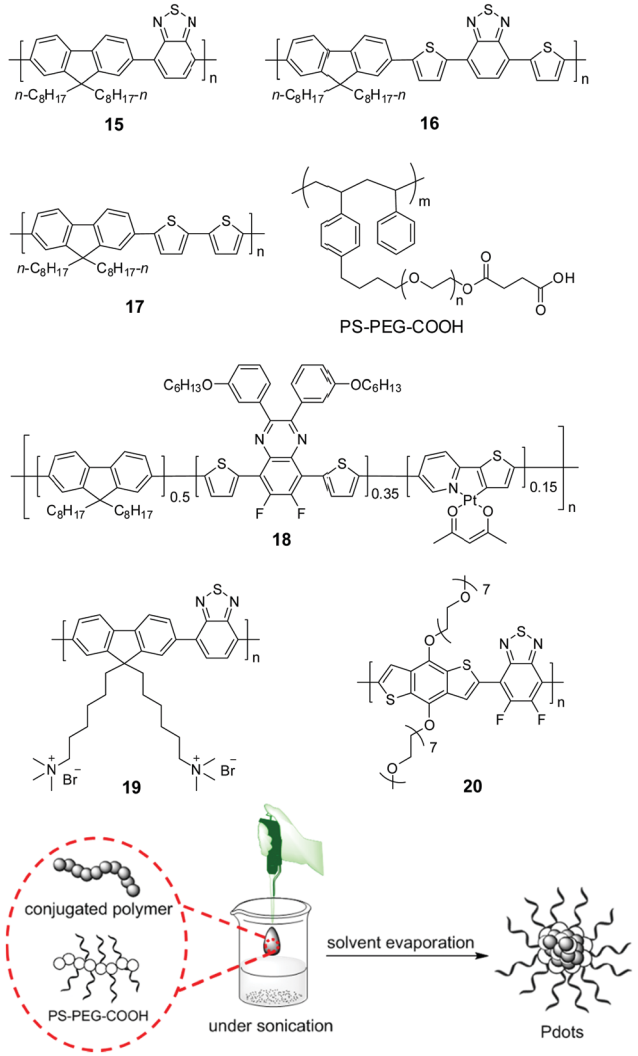

Fig. 6 Chemical structures of polymers **15–20** and preparation of polymer dots (Pdots) by the nano-precipitation method for photocatalytic H_2 production. The scheme is adapted with permission from ref. 82, Copyright 2016 Wiley-VCH.

Conjugated polyelectrolytes (CPEs) are a subclass of interesting water-soluble CPs with wide applications in photovoltaic devices, biomedical imaging and therapy, as well as biosensing, *etc.*[85–88] Their rigid conjugated structures endow them with excellent optoelectronic properties, while the hydrophilic side chains with charged groups allow for unique dispersibility of CPEs in polar solvents. We prepared cationic CPE **19** by one-step quaternization of the precursor polymer attaching a hexyl bromide side chain.[89] In the mixture of $Et_3N/CH_3OH/H_2O$, polymer **19** could self-assemble into homogeneous nanoparticles of ~180 nm. The suspension gives a HER of 512 μmol h^{-1} g^{-1}, which is 3-fold that of its counterpart without the side chain. The enhanced HER was attributed to the improved light absorption and charge separation of the nanoparticles.

Different from the cationic CPEs, attaching oligoethylene glycol (OEG) side chains endows polymer **20** with more interesting functions.[90] The O atom in the OEG side chain favours the interface contact of the polymer backbone with water, which resulted in a much smaller water contact angle of **20** (27.5°) than that of an alkyl-functionalized polymer (101.2°). Moreover, the side chains could interact with Pt, resulting in more efficient charge transport from the polymers to Pt. Polymer **20** loaded with 3 wt% Pt gave a HER of 12.8 mmol h^{-1} g^{-1}, which is much higher than its alkyl-attached counterpart.

Besides, soluble CPs could also be processed into films for photocatalytic H_2 production. By drop-casting, Cooper's group prepared a film of polymer **4** attaching a 2-ethylhexyl side chain. The film demonstrated a HER of 72 μmol h^{-1} g^{-1} when immersed in the $Et_3N/CH_3OH/H_2O$ mixture (>420 nm).[91]

3.1.2 Conjugated porous polymers. Crosslinked CPs with a three-dimensional porous feature have gained ever-increasing interest because of their large electron delocalized network structure, excellent stability and tunable optoelectronic properties. These advantages have stimulated their wide applications in energy storage, chemical sensing, gas absorption and storage, heterogeneous catalysis, *etc.*[50,92–95] In recent years, conjugated porous polymers (CPPs) have attracted good research interest in photocatalytic H_2 evolution. Their inherently porous structures can enhance the interaction between the polymers and water molecules and promote the charge transfer in different dimensions, which is expected to boost the photocatalytic reactions.[33,95]

The statistical copolymerization of aromatic monomers was reported as an important strategy to enhance the catalytic activity of CPPs by improving their physical properties such as band gap, porosity and charge mobility, *etc.* For instance, Cooper and co-workers synthesized fifteen conjugated microporous polymers (CMPs) by adjusting the feed ratio of the four comonomers shown in Fig. 7.[96] The CMPs have high surface areas of 597–1710 $m^2\ g^{-1}$ and their band gaps gradually decrease from 2.95 to 1.94 eV with the increase of pyrene content in the polymer. Without adding a metal cocatalyst, the polymers showed gradually enhanced HER when the band gap decreased from 2.95 to 2.33 eV. With the ratio of 1,4-benzene diboronic acid and 1,2,4,5-tetrabromobenzene of 2 : 1, polymer **21** exhibited the highest HER of 174 μmol $h^{-1}\ g^{-1}$. However, further narrowing the band gap of polymer led to a decrease in the H_2 production. This was likely ascribed to the increased nonradiative recombination of electron and hole in the pyrene-rich polymers.

Similarly, Jiang *et al.* synthesized D–π–A CPPs using pyrene as a donor, benzothiadiazole as an acceptor, and benzene or biphenyl as a π-crosslinker unit.[97] Compared to D–A polymers (without π unit), the extended π-conjugation endows the D–π–A polymers with more efficient charge migration to the surface of polymer particles. In addition, the electron push–pull interaction in the D–π–A polymer backbone could facilitate charge separation in the photocatalytic process. Thereby, D–π–A polymers exhibited better hydrogen production than the D–A and D–π–D polymers (without acceptor). When the ratio of pyrene to benzothiadiazole was 9 : 2, a maximum HER of 296 μmol $h^{-1}\ g^{-1}$ was obtained (> 420 nm). Xiang *et al.* developed a series of CPPs by copolymerizing 1,3,6,8-tetrabromopyrene and 3,8-dibromophenanthroline. A remarkable HER of 4200 μmol $h^{-1}\ g^{-1}$ was achieved by the polymer having a 3 : 1 ratio for 1,3,6,8-tetrabromopyrene and 3,8-dibromophenanthroline.[98] In addition, Wang *et al.* further modified polymer **21** by gradually replacing the benzene units in the polymer network with dibenzo[*b*,*d*]thiophene sulfone units.[99] They claimed that the sulfone unit could act as an electron-output "tentacle" to trap photogenerated electrons from polymers, which is beneficial for the proton reduction reaction. The HERs of the resulting polymers were significantly enhanced with increasing content of sulfone unit in the polymer. This molecular modification provided a maximum HER of 400 μmol h^{-1}.

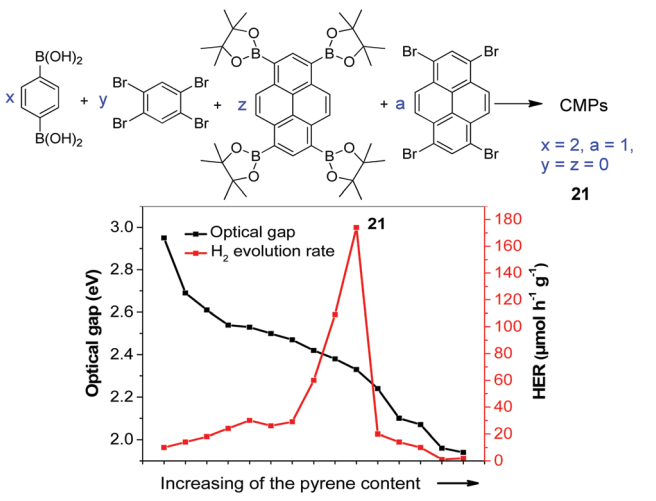

Fig. 7 Synthesis of conjugated microporous polymers with varying ratios of benzene and pyrene as well as the correlation of optical gap (red line) and hydrogen production (black line) as a function of increasing pyrene content in the polymer backbone.

The donor–acceptor combination approach is one of the most prevailing methods used in polymer solar cells to enhance the power conversion efficiency.[100–104] The alternating electron-rich donor (D) and electron-deficient acceptor (A) in the main chain could induce intramolecular charge transfer (ICT) interactions between D and A units, resulting in a narrowing of the band gap and molecular energy level modulation. Owing to this, the D–A approach has attracted a great deal of interest in designing CPs for photocatalytic H_2 evolution.

In 2016, Yu *et al.* reported CPPs by the combination of various chromophores (**M1**–**M4**) with biphenyl and bipyridyl, respectively.[105] With the chromophores from strong acceptors (**M1**) to strong donors (**M4**), the band gaps could be fine-tuned from 1.81 to 2.89 eV for **22a**–**25a**. The replacement of biphenyl (weak donor) with bipyridyl (weak acceptor) led to lower band gaps of 2.06–2.45 eV for **23b**–**25b** (Fig. 8a). The overall H_2 evolution of bipyridyl containing polymers is better than that of biphenyl containing polymers (Fig. 8b). Polymer **22b** gave the highest HER of 1900 μmol $h^{-1}\ g^{-1}$ (> 400 nm) as a result of the improved light absorption, wettability and charge separation. Later, a higher HER of 2590 μmol $h^{-1}\ g^{-1}$ was obtained by polymer **26** through further optimizing nitrogen-containing acceptors in **M4** based polymers.[106]

2,1,3-Benzothiadiazole (BT) is a strong acceptor unit used in designing D–A copolymers. Wang and co-workers demonstrated that the substitution position of BT on the central phenyl unit has a profound effect on the porosity and morphology of the resulting polymers.[107] CPPs with 1,2,4,5 and 1,2,4-substitution exhibited a fused particle-like shape and a fibre shape was observed for their counterpart with 1,3,5-substitution, while the BET surface areas of the three polymers ranged from **40** to 280 $m^2\ g^{-1}$ with optical gaps of 2.25–2.44 eV. Consequently, polymer **27** loaded with 3 wt% Pt yielded a HER of 400 μmol $h^{-1}\ g^{-1}$, while 8 μmol $h^{-1}\ g^{-1}$ and 26 μmol $h^{-1}\ g^{-1}$ were observed for the polymers with BT at the 1,2,4 and 1,3,5-positions of the central phenyl ring, respectively. Interestingly, compared to those 3D CPPs, a 1D linear

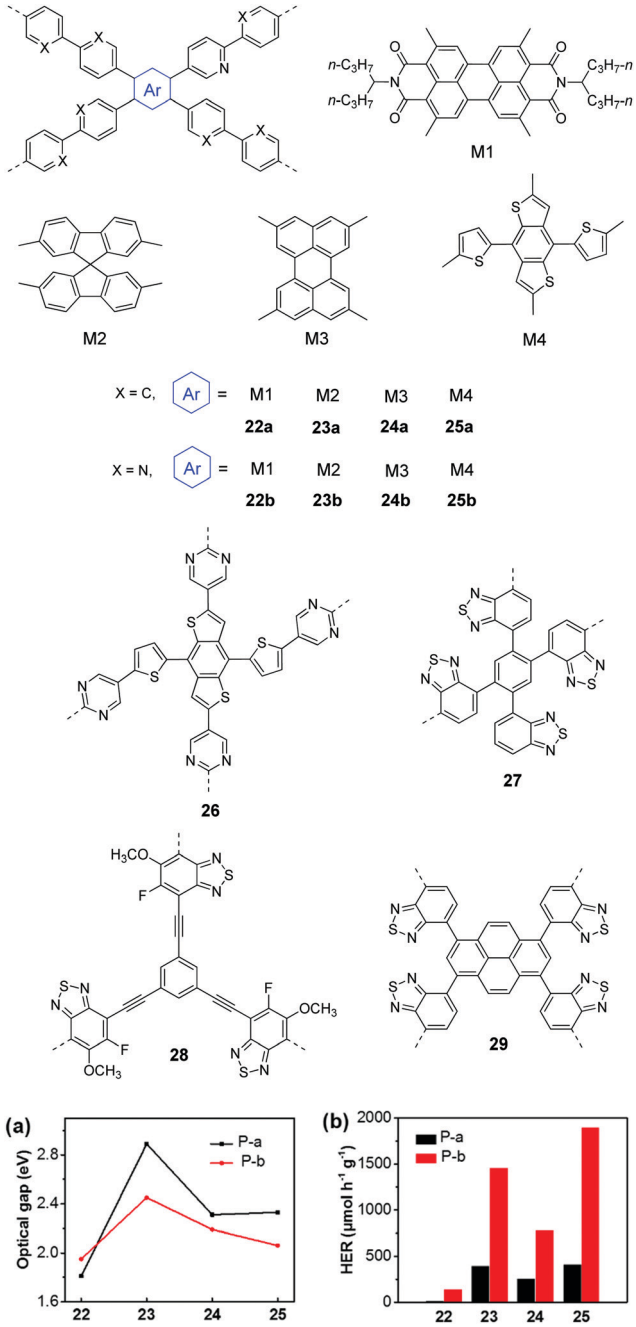

Fig. 8 Chemical structures of D–A type CPPs and (a) the optical gaps as well as (b) photocatalytic H_2 production of polymers **22–25** (P-a: **22a–25a**; P-b: **22b–25b**). Reprinted with permission from ref. 105. Copyright 2016 American Chemical Society.

polymer consisting of alternating phenyl and benzothiadiazole units showed a much higher HER of 2320 μmol h^{-1} g^{-1}, which was ascribed to its narrowest band gap (2.17 eV) and improved charge transport in the polymer.

Fluorine (F) substitution on the CP backbones is an effective way to engineer their optoelectronic properties.[108] The van der Waals radii of F atom is only 1.35 Å, which is close to that of the hydrogen atom (1.2 Å).[109] Besides, with a Pauling electronegativity value of up to 4.0, the F atom tends to impair the electron density in the D–A type CPs. As a consequence, the introduction of F does not cause a significant steric hindrance, but has a profound influence on the molecular orbits of the polymers.

Zhu and co-workers studied the F substitution effect in the case of BT incorporated linear CPs and conjugated porous polymers on their photocatalytic activities.[110] It was found that F substitution had a weak influence on the optical gaps of polymers but the charge transfer efficiency was improved significantly. With the increase of F atom number in BT from 0 to 2, the HOMO and LUMO levels of polymers decrease simultaneously. Polymer **28** incorporating CH_3O and F substituted BT units showed a HER of 9.6 mmol h^{-1} g^{-1}, which was 28.8-fold as large as that of its counterpart without fluorination. The F substitution was also examined by Wang and co-workers.[111] They found that the F substitution on BT led to a more negative LUMO level, which could increase the driving force for proton reduction. In this work, polymer **29** showed a 5-fold enhancement of HER compared to its non-fluorinated counterpart.

In general, extending the π-conjugation along the skeleton had multiple impacts on the morphologies, porous properties and photophysical properties of the resulting polymers, which have a synergistic effect on the photocatalytic performances of the CPs. For example, Zhang and co-workers examined the π-extended conjugation effect of polymers **30–33** on their H_2 production performances.[112] The spacer change led to a profound effect on the porosity of the polymers. Polymer **30** with a small *para*-phenylene spacer has micropores, while both micro- and mesopores were found for **31** and **33** with a longer spacer. By contrast, polymer **32** showed a much broader pore size distribution, which was due to the longest polyphenylene spacer in the polymer network. As a result, the BET surface areas were 669, 750, 564, and 834 m^2 g^{-1} for **31**, **32**, **33**, and **34**, respectively. In addition, the four polymers showed different energy level alignments due to the donor (arene units) and acceptor (tricyanomesitylene) interactions (Fig. 9a). The HERs were found to be 134, 598, 908, and 620 μmol h^{-1} g^{-1} for **30**, **31**, **32**, and **33**, respectively. Despite the similar band gap, the highest photocatalytic activity of **33** as compared to **30** and **31** was ascribed to its nanoparticle morphology and the largest surface area.

Similarly, Jiang *et al.* developed polymers **34–36** by changing the central π-linker from benzene to *p*-terphenyl.[113] Because of the higher steric hindrance of the biphenyl than phenyl, **34** showed a smaller BET surface area of 811 m^2 g^{-1} than **35** (915 m^2 g^{-1}), while **36** with the longest linker showed the lowest surface area of 447 m^2 g^{-1} (Fig. 9b). Moreover, the introduction of the extended linker seemed to favour the formation of larger pores. The three polymers showed a similar pore distribution but more mesopores or macropores were found for **35** and **36** (Fig. 9c). In addition, polymer **34** has a smaller band gap of 2.53 eV than **35** (2.62 eV) and **36** (2.64 eV). Polymer **34** exhibits better charge separation efficiency as evidenced by a much lower emission than that of **35** and **36** (Fig. 9d). Accordingly, polymer **34** yielded the highest HER of 2460 μmol h^{-1} g^{-1}, while HERs of 188 and 116 μmol h^{-1} g^{-1} were obtained by **35** and **36**, respectively.

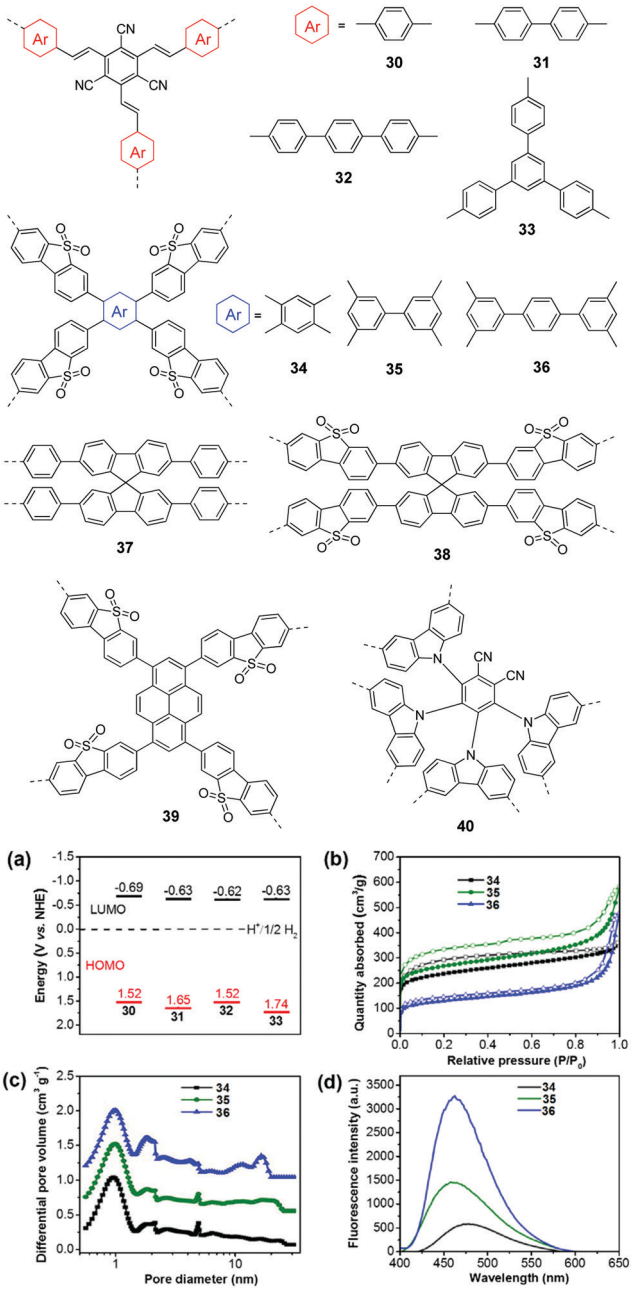

Fig. 9 Chemical structures of polymers **30–40**. (a) HOMO and LUMO band positions of polymers **30–33**. (b) Nitrogen sorption isotherms, (c) photoluminescence spectra, and (d) hydrogen evolution of polymers **34–36**. Reprinted with permission from ref. 112 and 113. Copyright 2017 Wiley-VCH and 2016 American Chemical Society.

Cooper *et al.* found that the optical gaps of the CMPs could be tuned by changing the monomer linker length and type of linkage, which led to different H_2 evolution activities.[114] With spirobifluorene as the core, polymer **37** exhibited a 15-fold HER as compared to that of the analogue with phenyl as the core. In addition, by extending the central core from phenyl to spirobifluorene, polymer **38** was reported with an improved HER of 3106 μmol h^{-1} g^{-1}.[115]

Jiang *et al.* demonstrated that the substitution position of dibenzo[*b*,*d*]thiophene sulfone had a significant influence on the photocatalytic performances.[116] They prepared two CMPs by linking pyrene at the 3,7 and 2,8 positions of sulfone, respectively. Polymer **39** with the 3,7-linking pattern showed a narrower optical gap and lower emission intensity than the other polymer, which indicated better photogenerated charge migration and thus led to a much higher HER of 8523 μmol h^{-1} g^{-1} than that of the 2,8-linked polymer (2650 μmol h^{-1} g^{-1}). Similarly, Su and co-workers found that substitution positions of CN groups and carbazole on the central phenyl ring could affect spectral absorption and charge separation of the resulting polymers. With an optimized structure, polymer **40** showed an excellent HER of 2103.2 μmol h^{-1} g^{-1} and 6.4% apparent quantum yield at 420 nm.[117]

3.1.3 Covalent organic frameworks. Covalent organic frameworks (COFs) are an emerging class of 2D or 3D crystalline polymers formed by linking organic building units into extended structures.[47,49,51,118] The high degree of crystallinity favours charge separation and transport, which endows COFs with promising catalytic activity. Moreover, the well-defined pores, excellent stability and fine-tuned physicochemical properties of COFs make them attractive photocatalysts for H_2 production.

In an early contribution, Lotsch *et al.* synthesized COF **41** (TFPT-COF) by a condensation reaction of 2,5-diethoxyterephthalohydrazide and 1,3,5-tris(4-formylphenyl)triazine in a 1,4-dioxane/mesitylene mixture.[119] COF **41** showed a honeycomb-type layered structure with mesopores of 3.8 nm and its BET surface area was up to 1603 m^2 g^{-1}. Pt-loaded COF **41** could produce H_2 from water at a constant rate of 1970 μmol h^{-1} g^{-1}. Subsequently, they reported a series of azine-linked COFs **42–45** (N_x-COFs, x = 0–3) with different *N* numbers in the central aryl ring (Fig. 10).[120] The molecular design is based on the varied dihedral angles between the central aryl ring and peripheral phenyl rings by replacing the H atom (green dots) with a N atom (Fig. 11a), which led to different planarity of the platform and thus varied crystallinity and porosity of the resulting COFs. As displayed in Fig. 11b, compared to **42** (N_0-COF) and **43** (N_1-COF), **44** (N_2-COF) and **45** (N_4-COF) have better crystallinity as revealed by their sharper PXRD peaks, which is beneficial for charge migration in the photocatalytic reaction. Besides, the four COFs showed close band gaps of 2.6–2.7 eV, but different BET areas of 326 to 1536 m^2 g^{-1}. The HERs of Pt-modified **42**, **43**, **44** and **45** were 23, 90, 438 and 1703 μmol h^{-1} g^{-1}, respectively. The progressively enhanced HER was likely attributed to the increased surface area and improved charge migration when the number of N atoms was increased in the frameworks.

The facile choice of building blocks did permit a good modulation of the porosity, wettability and optoelectronic properties of β-ketoenamine linked COFs, which led to enhanced photocatalytic performance. When different building blocks were introduced, the corresponding band gaps were 2.10, 1.85 and 2.28 eV for **46** (F-COF), **47** (FS-COF) and **48** (TP-COF), respectively (Fig. 11c).[121] Moreover, **46** and **47** containing a sulfone unit exhibited better wettability than **48** as revealed by the water contact angle measurement, which facilitates dispersion of COF particles in water and the interaction between COF and water in the photocatalytic reaction. Loaded with 3 wt% Pt,

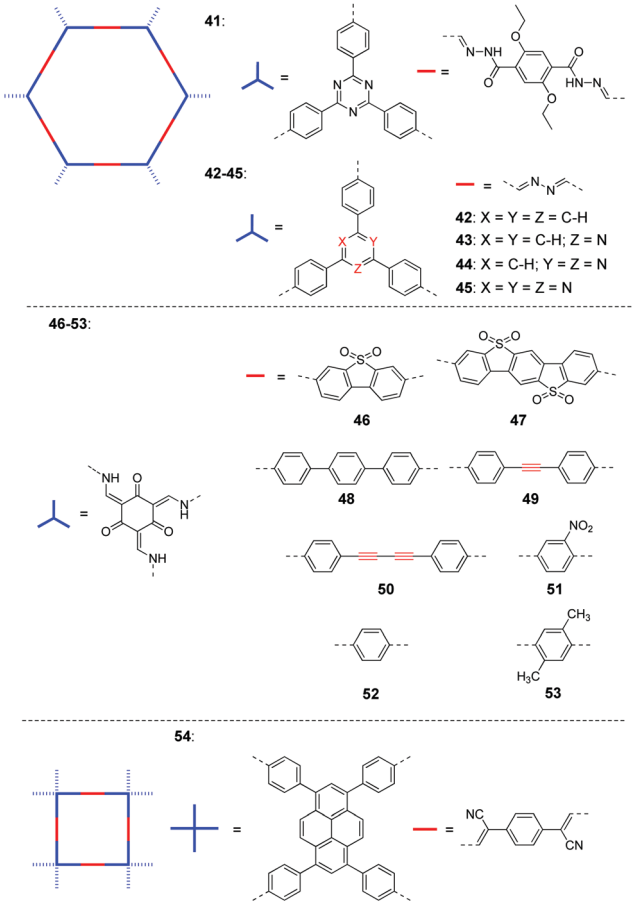

Fig. 10 Chemical structures of COFs **41–54** for photocatalytic H_2 production under visible light.

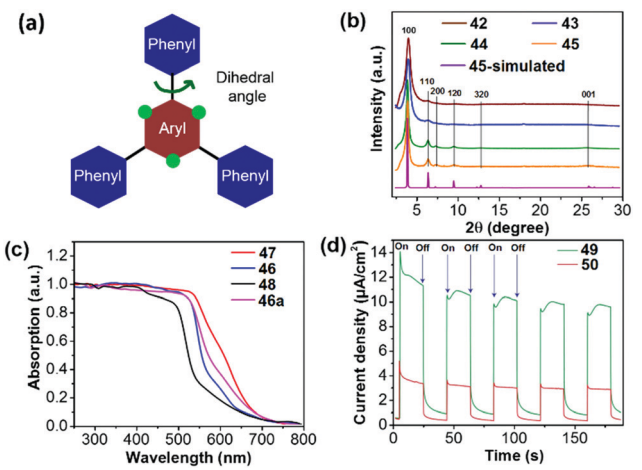

Fig. 11 (a) Design principle and (b) PXRD patterns of COFs **42–45**. (c) Diffuse reflectance spectra of COFs **46–48** (**46a** is an amorphous analogue of **46**). (d) Transient photocurrent for COFs **49** and **50** measured in 0.5 M KCl solution under visible light irradiation. Reprinted with permission from ref. 120–122. Copyright 2015 Nature Publishing Group, 2018 Nature Publishing Group and 2018 American Chemical Society.

the HER of **46** was up to 4.44 mmol h^{-1} g^{-1}, while 10.1 and 1.6 mmol h^{-1} g^{-1} were reached for **47** and **48**, respectively. The best H_2 evolution of **47** was ascribed to its lowest band gap, good wettability, highest BET area (985 m^2 g^{-1} for **46**, 1288 m^2 g^{-1} for **47** and 919 m^2 g^{-1} for **48**).

In addition, the photocatalytic activity of COFs is susceptible to linking bond length between comonomers. Thomas and co-workers reported that the catalytic activity of the diacetylene-based COF **49** (TP-EDDA) was much better than the acetylene-based COF **50** (TP-BDDA).[122] Despite the almost identical band gaps (2.34 eV for **49** and 2.31 eV for **50**), COF **50** has an HER of 324 μmol h^{-1} g^{-1}, whereas a relatively low HER of 30 μmol h^{-1} g^{-1} was achieved for **49**. The significantly enhanced HER was attributed to the higher charge carrier generation of **50** under visible light, which could be revealed by the larger photocurrent response of **50** as shown in Fig. 11d.

Substituent modification in the COF could also bring good photocatalytic performances. Sun *et al.* prepared three ketoenamine-based COFs (**51–53**) and studied the effect of different functional groups on their photocatalytic activities.[123] The photocurrent density of COF **53** (TpPa-COF-$(CH_3)_2$) is about 2.3-fold and 6.5-fold higher than that of **52** (TpPa-COF-H) and **51** (TpPa-COF-NO_2), respectively. Moreover, the electron transfer resistance value decreased gradually when the electron-donating ability of the substituent groups became stronger (from NO_2 to H, then CH_3). These results indicated that the charge separation of COFs was improved by increasing the electron-donating properties of the substituents. With an optical gap of 2.06 eV and the best charge separation efficiency, COF **52** showed a HER of 8.33 mmol h^{-1} g^{-1}, which was much higher than that of **51** (1.56 mmol h^{-1} g^{-1}) and **53** (0.22 mmol h^{-1} g^{-1}).

In comparison with those reported COFs based on imine-, hydrazone-, or azine linkers, fully π-conjugated COFs are expected to allow for more efficient exciton separation and migration over the framework, which is good for H_2 production. Very recently, Jiang and co-workers reported a 2D sp^2 carbon-COF **54** (sp^2c-COF) as the H_2-producing photocatalyst, into which electron-withdrawing cyano groups were incorporated to impart a conjugated electron donor–acceptor structure and the phenylenevinylene further improved π conjugation.[124] The BET surface area of COF **54** was 602 m^2 g^{-1} and its optical gap was 2.05 eV. A stable HER of 1360 μmol h^{-1} g^{-1} was obtained under visible light. The HER could be enhanced to 2120 μmol h^{-1} g^{-1} by attaching 3-ethylrhodanine as an end-capping group to strengthen the push–pull effect.

3.1.4 Covalent triazine frameworks. As another class of organic framework materials, covalent triazine frameworks (CTFs) are featured by unique porosity and high nitrogen content, which could be obtained by the choice of suitable organic linkers and synthetic conditions. Different from COFs, most of CTFs reported so far are amorphous or semicrystalline. Recently, CTFs have been employed for a range of applications, such as CO_2 capture and storage, photocatalysis and energy storage.[53,125–127]

In 2015, Wu and co-workers prepared CTF **55** (CTF-T1) by a trimerization reaction of terephthalonitrile using CF_3SO_3H as the catalyst at room temperature (Fig. 12).[128] The CTF exhibits a band gap of 2.94 eV and a low HER of 200 μmol h^{-1} g^{-1} after loading 3 wt% Pt.

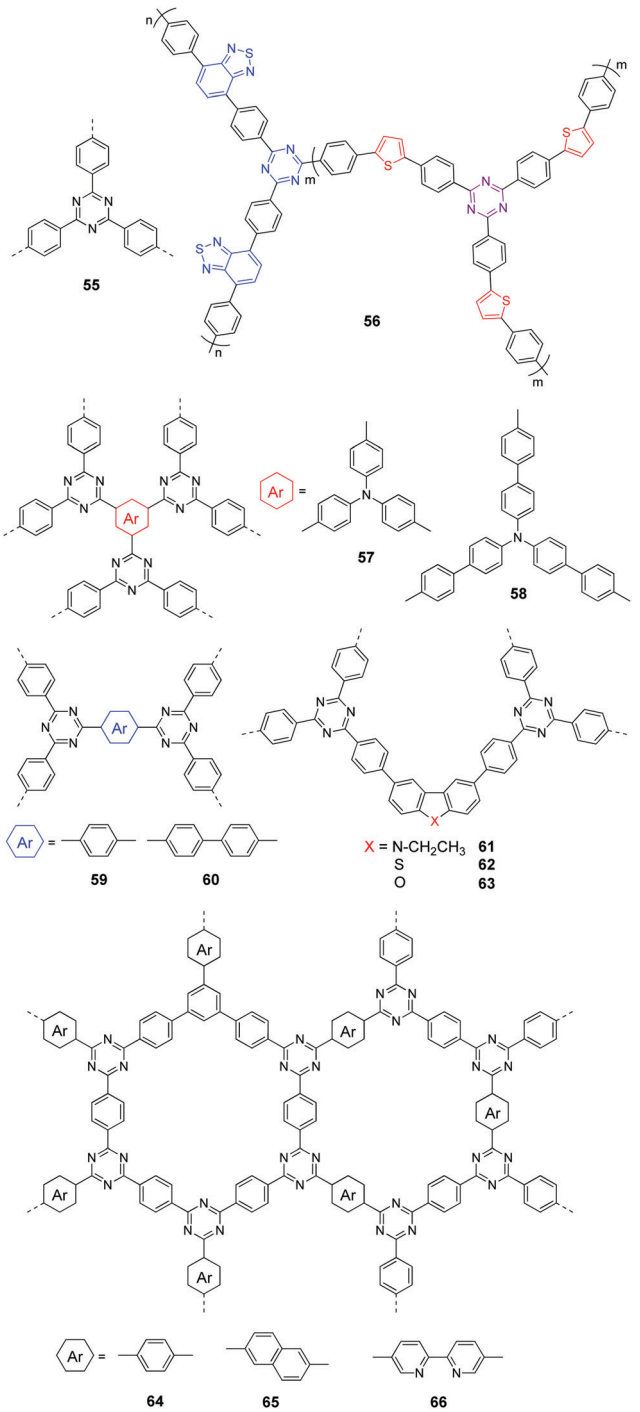

Fig. 12 Chemical structures of polymers **55–66**.

Afterward, Thomas *et al.* showed that a CTF with a low HER could be converted into a more efficient photocatalyst by further mixing the pre-synthesized CTF in $CHCl_3/CF_3SO_3H$ with $ZnCl_2$ salt for 10 minutes. The HER could increase from 186 to 1072 μmol h^{-1} g^{-1} due to the decreased optical gap (2.42 eV) and improved crystallinity.[129] Alternatively, Wang *et al.* further processed the pre-synthesized CTF **55** through thermal annealing at 300 °C, which induced structural reorganization of **55** and yielded new conjugated heterocycles in the polymer. With improved light absorption and charge mobility, 3 times enhancement of HER was achieved under visible light as a result of the thermal treatment of **55**.[130]

The fast recombination of photogenerated electrons and holes of CTFs is another major disadvantage preventing them from achieving higher efficiencies. In this context, Li *et al.* developed a molecular heterostructure **56** (CTF-Th) *via* a two-step synthetic strategy.[131] CTF **56** exhibited higher photocurrent and charge carrier density than its single-component counterparts, which suggested a largely improved charge separation efficiency. As a result, a HER of 6.6 mmol h^{-1} g^{-1} was obtained for **56** under visible light.

Compared to the commonly used ionothermal method (usually at 400 °C), polycondensation under relatively gentle conditions is desirable for the preparation of CTFs with tunable functions and geometries. Tan and co-workers developed CTFs **57–60** by condensation between 1,4-benzenedicarboximidamide and different aldehydes in the presence of Cs_2CO_3.[132] The structural variations have an obvious impact on the porosity and light absorption of the resulting CTFs. The BET surfaces areas are 807, 764, 663, and 757 m^2 g^{-1} for **57** (CTF-HUST-3), **58** (CTF-HUST-3), **59** (CTF-HUST-1) and **60** (CTF-HUST-2), respectively (Fig. 13a). CTFs **57** and **58** showed broader absorption compared to **59** and **60** (Fig. 13b). Under visible light, CTF **60** showed the highest HER of 2647 μmol h^{-1} g^{-1}, while the HERs were 1238, 1582 and 1460 μmol h^{-1} g^{-1} for **57**, **58** and **59**, respectively. Using a similar synthetic method, Tan *et al.* prepared donor–acceptor CTFs **61–63**.[133] Upon incorporating a strong electron-donating carbazole unit, **61** (CTF-N) showed the lowest band gap of 2.17 eV compared to **62** (CTF-S, 2.47 eV) and **63** (CTF-O, 2.67 eV) (Fig. 13c). Meanwhile, the enhanced charge separation/transfer efficiency of **61** was studied by employing fluorescence and photoelectrochemical measurements (Fig. 13d). Therefore, CTF **61** decorated with 3 wt% Pt exhibits the best HER of 10 760 μmol h^{-1} g^{-1}.

CTFs could also be fabricated by a Pd-catalyzed coupling reaction. In 2017, Cooper *et al.* synthesized two series of CTFs with similar structures by either Suzuki coupling of 2,4,6-tris-(4-bromophenyl)-1,3,5-triazine and aromatic monomers or trimerization of dicyanobenzene derivatives.[134] In this case, Pt loaded CTFs from trimerization exhibited higher activity than their counterparts from Suzuki coupling. Moreover, the length of the *para*-phenylene spacer has a profound effect on the band gaps and porosity for both series of CTFs and thus affects their photocatalytic activities. Based on the D–A interaction between thiophene derivatives (donor) and triazine units (acceptor), Bojdys *et al.* designed eight CTFs with fine-tuned band gaps (2.06–2.70 eV) and charge transfer in the polymer.[135] As a result, a maximum HER of 3158 μmol h^{-1} g^{-1} was achieved by the CTF consisting of benzotrithiophene and triazine.

Instead of introducing different building blocks into CTFs, heteroatom doping is another efficient method to boost the HERs of CTFs. Su *et al.* prepared S-doped CTF samples ($CTFS_{10}$) by annealing treatment of CTFs with sulfur.[136] The S concentration in the framework was 0.5–0.52 atom% when the CTF was mixed with different amounts of S (5–30 wt%). The characteristic peak of C–S at 286.5 eV revealed by XPS analysis showed that the

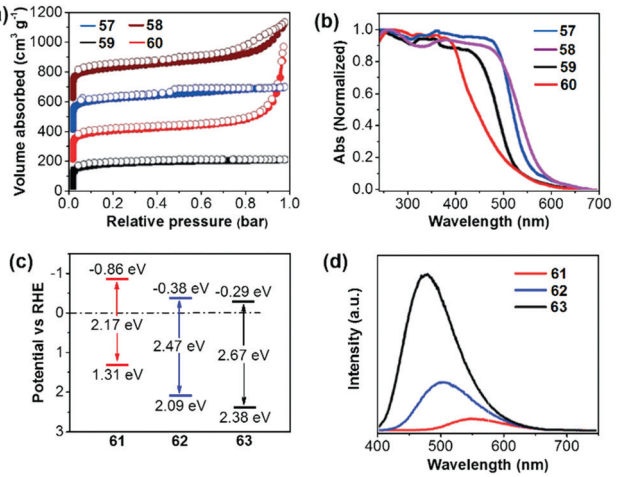

Fig. 13 (a) Nitrogen sorption curves and (b) UV-vis absorption spectra of CTFs **57–60**. (c) Energy diagram and (d) fluorescence spectra of CTFs **61–63**. Reproduced with permission from ref. 132 and 133. Copyright 2017 Wiley-VCH and 2018 Royal Society of Chemistry.

S atom is covalently bound to the CTF backbone. After depositing 3 wt% Pt, the CTFs mixed with 10 wt% S showed the best HER of 2000 μmol h^{-1} g^{-1}, which is 5-fold enhanced compared to that of the pristine CTFs. This is due to the sharply decreased band gap (from 2.87 eV to 1.87 eV) and improved charge transport after S doping. Alternatively, the photocatalytic activity of CTFs could be enhanced by phosphorus doping due to the narrower band gap and more efficient charge transfer.[137]

Besides the above-mentioned amorphous CTFs, Tan and co-workers reported the successful preparation of crystalline CTFs **64–66** by *in situ* oxidizing alcohols into aldehyde monomers and studied their H_2 production activities.[138] It was claimed that high crystallinity of CTFs could be achieved by slowing down their nucleation process through controlling aldehyde monomer generation in the polycondensation reaction. All CTFs showed good crystallinity with BET surface areas of 520–599 m^2 g^{-1}. The HERs of **64** (CTF-HUST-C1), **65** (CTF-HUST-C5) and **66** (CTF-HUST-C6) were 5100, 2400 and 650 μmol h^{-1} g^{-1}, respectively. In addition, Zou and co-workers prepared crystalline CTFs by condensation of melamine (MA) and pyromellitic dianhydride (PMDA) under thermal conditions. The obtained CTF displayed a band gap of 2.7 eV and HER of 7 μmol h^{-1}.[139]

3.1.5 Carbon nitrides. Pure g-C_3N_4 materials have an optical gap of about 2.7 eV and suitable CB/VB positions for water reduction and oxidation. g-C_3N_4 has captured broad research interest toward photocatalytic H_2 evolution since the pioneering report by Wang and co-workers in 2009.[140] The photocatalytic activity of g-C_3N_4 has subsequently been improved by morphology modulation, crystallinity control, doping and composite construction, *etc.*[29–35,141] Given the fact that these developments have been summarized in previous reviews,[29–35,141] this section briefly presents the representative research on molecular modification of g-C_3N_4 photocatalysts for H_2 production from water.

The elemental doping strategy has been intensively developed to boost the photocatalytic performance of g-C_3N_4 by tuning its band structure, light absorption and charge carrier transport.[27–32]

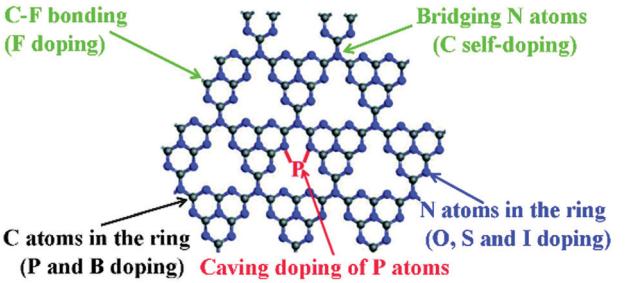

Fig. 14 Possible elemental doping sites in the single layer of g-C_3N_4. Reproduced with permission from ref. 141. Copyright 2017 Royal Society of Chemistry.

Various elements such as F, Br, I, N, P, O, S and B have been doped in the skeleton of tri-*s*-triazines based g-C_3N_4, as shown in Fig. 14.[141] For instance, Wang *et al.* prepared F doped g-C_3N_4 (CN–F) by adding NH_4F in the polymerization of dicyanamide. The formation of C–F bonds in the polymer led to a slightly red-shifted optical absorption and 2.7 times higher HER (~130 μmol h^{-1} g^{-1}) than that of the unmodified sample (>420 nm).[142] Nitrogen-doped g-C_3N_4 (CN–N) could be synthesized using pre-treated melamine with hydrazine hydrate.[143] This modification gave rise to improved charge transfer and a slightly narrowed band gap from 2.72 eV to 2.65 eV, as a result, CN–N showed a 1.8-fold higher HER of 553.5 μmol h^{-1} g^{-1} than that of pristine g-C_3N_4 (>400 nm). On the other hand, the doping of multiple elements in g-C_3N_4 provided more variable properties.[141] Dai *et al.* reported carbon and phosphorus co-doped g-C_3N_4 (CN–C/P), which showed a significantly larger surface area of 141.1 m^2 g^{-1} than pristine g-C_3N_4 (24.9 m^2 g^{-1}).[144] Moreover, this modulation also led to extended optical absorption and promoted charge transfer in the polymer. Benefiting from this, CN–C/P exhibited a HER of 1493.3 μmol h^{-1} g^{-1}, which was 9.7-fold as compared to that of pristine g-C_3N_4.

Organic small molecules are also capable of doping into g-C_3N_4 by copolymerization to adjust its π-electronic system and band structure. In 2010, Wang and co-workers prepared modified g-C_3N_4 (CN–BA) using dicyandiamide and barbituric acid as the precursor and dopant, respectively.[145] With an optimization of amount of dopants, CN–BA exhibited a maximum HER of 294 μmol h^{-1} g^{-1} mainly due to the extended light absorption. After that, many other small molecules such as pyrimidine,[146] quinoline,[147] and thiophene[148] were incorporated into g-C_3N_4 by several groups.

Structure defect engineering is another efficient approach for improving the photocatalytic performance of g-C_3N_4. The introduction of defects into the g-C_3N_4 backbone can not only modify the band structure by generating mid-gap states to extend the light absorption, but also act as trapping sites for charge carriers to inhibit the recombination of electrons and holes. In the presence of KOH, Zhang *et al.* introduced nitrogen vacancies and cyano groups into g-C_3N_4, which resulted in a reduced band gap from 2.68 to 2.36 eV and enhanced charge carrier separation.[149] Therefore, the defect-rich g-C_3N_4 showed a HER of 6.9 mmol h^{-1} g^{-1}, which was nearly twice that of pristine g-C_3N_4. In a very recent study, Wang *et al.* introduced

defects into g-C_3N_4 by $NaBH_4$ reduction of a crystalline pristine polymer under an inert atmosphere, which achieved nearly 8 times higher HER than the pristine polymer.[150] Apart from those modification strategies, the development of analogous polymers of g-C_3N_4 such as $C_3N_3S_3$[151] offered new opportunities for exciting findings in photocatalytic H_2 production.

In some cases, the construction of polymer heterojunctions (PHJs) can efficiently modulate the band structure and charge transport of g-C_3N_4 through inter/intramolecular π–π interactions between g-C_3N_4 and the aromatic structures. Shen *et al.* prepared three PHJs by coating different polyfluorene polymers on the surface of g-C_3N_4, which resulted in extended optical absorption and promoted charge transfer within the PHJs.[152] Under visible light, all three pure CPs have no photocatalytic activity and pure g-C_3N_4 showed a very low HER of 87.4 μmol h^{-1} g^{-1}. Among the three PHJs, 5% polymer **15** coated g-C_3N_4 (CN–P15) exhibited a maximum HER of 722.2 μmol h^{-1} g^{-1}. Using a similar method, Chen *et al.* deposited Pdots on the surface of g-C_3N_4 nanosheets, which yielded an enhanced HER *via* improved charge transfer from Pdots to g-C_3N_4 nanosheets.[153] In this case, 5 wt% polymer **17** deposited PHJ (CN–P17) exhibited a HER of 929.3 μmol h^{-1} g^{-1}, which is higher than that of its counterpart coated with polymer **15** (439.6 μmol h^{-1} g^{-1}). Besides, Wang *et al.* fabricated type II heterojunctions by anchoring pyrene-based polymers onto CN to improve light absorption and interface charge transfer.[154] By optimizing the amount and molecular structures of polymers, CN–PyP hybrids attained a maximum HER of 600 μmol h^{-1} g^{-1} without Pt deposition. PHJs based on g-C_3N_4 could also be prepared by linking another component through a chemical bond. Yan *et al.* prepared heterojunctions (CN–COF) by *in situ* formation of a COF on the surface of pre-synthesized g-C_3N_4 through condensation of amino group in g-C_3N_4 and aldehyde group in the COF.[155] CN–COF attained a dramatically enhanced HER of 10.1 mmol h^{-1} g^{-1}, which is much higher than those of the pure COF (0.16 mmol h^{-1} g^{-1}), g-C_3N_4 (1.05 mmol h^{-1} g^{-1}) and their mixture (0.93 mmol h^{-1} g^{-1}). Zou and co-workers fabricated heterostructured photocatalysts (CN–CTF) by linking g-C_3N_4 and CTFs with amide bonds, which demonstrated a good HER of 850 μmol h^{-1} g^{-1} and high stability compared to their counterpart (CN and COFs connected *via* van der Waals forces).[156] These investigations offer more opportunities for the design of H_2-production polymer photocatalysts. The photocatalytic activity and stability of these materials remain a great concern.

3.1.6 The role of the Pt cocatalyst and residual Pd on photocatalytic H_2 production of CPs. As shown above, noble metals were commonly deposited as cocatalysts on the surface of polymer materials to promote their H_2 production activities. The deposition of noble metal cocatalysts can effectively lower the overpotential or activation energy for proton reduction reactions. Moreover, the cocatalysts could act as charge trap centre to extract more electrons from the polymer photocatalysts, which favours the electron–hole separation at the cocatalyst/polymer interface.[157–159] Notably, as early as 1990s, Yanagida *et al.* have found that the catalytic activity of linear CPs could be improved by loading Ru nanoparticles.[67–69]

Among the commonly used metal cocatalysts such as Ru, Pd, Rh, Au, and Ag, Pt is a versatile cocatalyst mainly because of its largest work function for trapping photogenerated electrons and lowest overpotential for photocatalytic H_2 evolution.[158] In general, Pt is deposited on CPs by photoreduction of H_2PtCl_6 in the reaction system. Under light illumination, Pt(VI) is reduced by the photo-induced electrons of the polymer to produce Pt(0) nanoparticles with sizes of 3–5 nm *in situ* on the polymer surface. Compared to the pristine polymer, the Pt–polymer composite exhibited greatly enhanced H_2 evolution. H_2PtCl_6 with a Pt mass concentration of 3 wt% was commonly used in the photodeposition experiment, because too low Pt concentration provided only a few active sites for proton reduction, which resulted in a low enhancement of catalytic activity. Excessive amount of Pt deposited on the surface of the polymer photocatalyst could prevent light absorption by shielding the incident light and stimulate the aggregation of Pt nanoparticles, which is detrimental to the activity of Pt.

Pd-catalyzed cross-coupling polymerization reactions are widely used to synthesize CPs for photocatalytic water splitting. Residual Pd inevitably existed in the polymer and may play a vital role in its photocatalytic process.[160] Yu *et al.* have shown that the Pd content in the porous polymer greatly affected the H_2 evolution.[105] By changing the initial feeding ratio of $Pd(PPh_3)_4$ and monomer from 0.005 to 0.40, the Pd content was increased from 0.04% to 1.88% as measured by inductively coupled plasma mass spectrometry (ICP-MS). As shown in Fig. 15a, the HER of polymer **25b** was sharply improved with increasing Pd content from 0.04% to 0.46%, which became saturated at a higher residual Pd content. In addition, upon loading with 2 wt% Pt, a ~5-fold enhancement of the AQY at 350 nm was measured for **25b** (Fig. 15b), which verified the importance of the Pt cocatalyst in the enhancement of photoactivity.

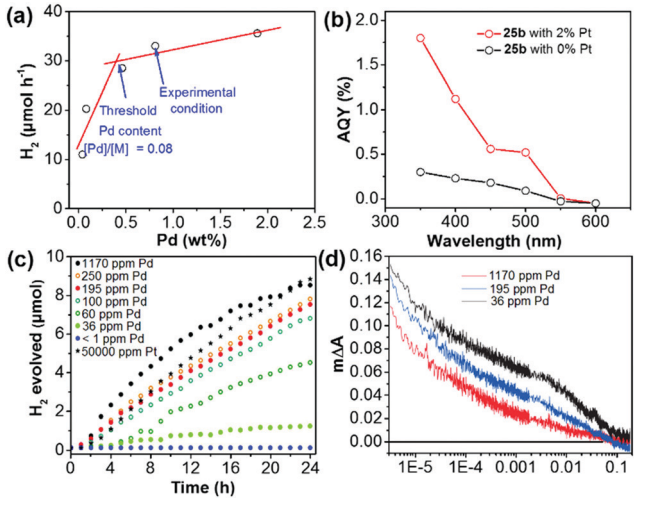

Fig. 15 (a) H_2 evolution of polymer **25b** with different residual Pd contents. (b) Apparent quantum yield (AQY) of polymer **25b** with 2% and without Pt loading at different wavelengths. (c) H_2 evolution of nanoparticles of polymer **15** with different amounts of Pd or Pt. (d) Transient kinetics of nanoparticles of polymer **15** with different Pd concentrations in a diethylamine/water mixture. Reprinted with permission from ref. 105 and 161. Copyright 2016 American Chemical Society and 2018 Wiley-VCH.

To study the role of Pd residues in determining the H_2 evolution activity, Jan Kosco and co-workers prepared colloidal polymer **15** nanoparticles with different Pd contents.[161] In the sample preparation, they first purified the as-prepared polymer **15** by gel permeation chromatography (GPC), and then washed the polymer with diethyldithiocarbamate. After the treatment, the Pd content in polymer **15** was below 1 ppm and the content could be gradually adjusted to 1170 ppm by adding $Pd_2(dba)_3$ solution. Fig. 15c displays that the H_2 evolution of nanoparticles of polymer **15** is gradually enhanced with increasing Pd content from <1 ppm to $\sim$100 ppm, at which point the evolved H_2 begins to saturate. Transient absorption spectroscopy (TAS) suggested that Pd could mediate electron transfer from the nanoparticles of polymer **15** to protons in the reaction media (Fig. 15d). It was found that photogenerated electrons were increasingly accumulated with decreasing Pd content in nanoparticles of polymer **15**. This indicates that the Pd cocatalyst could effectively suppress the accumulation of long-lived electrons and thereby accelerate photocatalytic H_2 generation of polymer **15**.

3.2 Conjugated polymers for photocatalytic O_2 evolution

The photocatalytic O_2 evolution is a critical step in water splitting because the four-electron transfer is an uphill process with large overpotentials and slow kinetics, which makes it very challenging to develop robust photocatalysts for water oxidation.[162,163]

To date, most of the O_2 evolution photocatalysts have been based on nitrogen-rich CPs. In 2017, Xu *et al.* reported polymer **67**, which has a nanosheet morphology and a very low band gap of $\sim$1.22 eV.[41] With $AgNO_3$ as the electron scavenger, **67** exhibits an oxygen evolution rate (OER) of 1.0 μmol h^{-1}, which could be enhanced to 14.3 μmol h^{-1} after loading $Co(OH)_2$ as the cocatalyst. More interestingly, polymer **67** can catalyze water oxidation under near-infrared light ($>$800 nm) and the OER is $\sim$0.4 μmol h^{-1} while g-C_3N_4 is not active.

Inspired by the facile tunability of CTFs, Wang *et al.* synthesized polymers **68–70** with different numbers of phenyl units in the polymer backbone.[164] The band gaps of **68–70** decreased from 2.98 eV to 2.36 eV with increasing number of phenyl units (Fig. 16a). Importantly, their HOMO/LUMO levels straddle the potential of water splitting, suggesting sufficient driving force for both photocatalytic water reduction and oxidation. Furthermore, both the HOMO and LUMO levels decreased with the increase of phenyl number in the polymer. After loading with 3 wt% $Co(NO_3)_2$ as a cocatalyst, polymer **69** showed the highest OER of 3 μmol h^{-1} ($>$300 nm) compared to **68** ($\sim$1 μmol h^{-1}) and **70** ($\sim$0.4 μmol h^{-1}) in the presence of $AgNO_3$, which was attributed to the synergistic effect of improved light absorption and charge transfer. In addition, the catalytic activity of **69** is also much better than that of C_3N_4 (Fig. 16b) due to the lower LUMO position of **69**. Notably, polymer **69** could produce 7.2 μmol of O_2 after 8 h visible-light irradiation. Considering that high crystallinity of CTF materials is desirable for exciton separation and thus enhancing the photocatalytic activity, Tang and co-workers reported highly ordered CTFs made by microwave-assisted polymerization.[165] The crystallinity of the resulting CTFs became higher with the increase of microwave

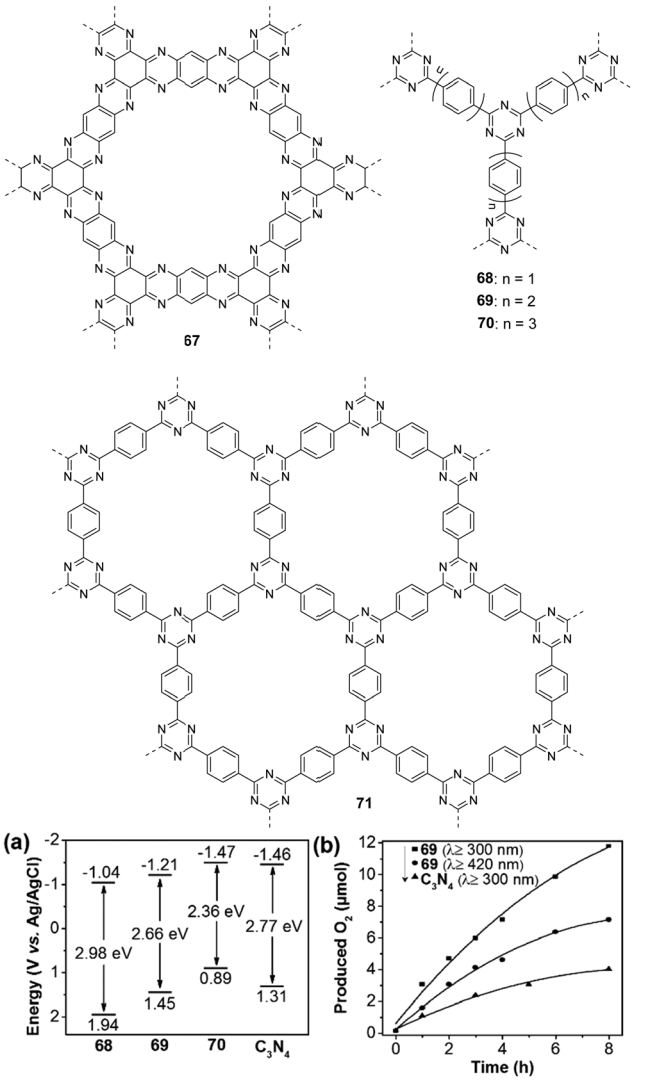

Fig. 16 Chemical structures of polymers **67–71**; (a) band structure diagram and (b) time course of the O_2 production for polymer **69** and C_3N_4. Reprinted with permission from ref. 164. Copyright 2018 Wiley-VCH.

power from 20 to 100 W. However, a further increase in microwave power can destroy the hexagonal units. At a power of 100 W, polymer **71** has a well-defined planar structure as evidenced by a G^+ peak at 1613 cm^{-1} from the Raman spectra analysis of CTFs. In addition, polymer **71** has conduction band (CB)/valence band (VB) levels of −0.74/+2.18 eV (*vs.* NHE, pH = 0), which is suitable for the photocatalytic water oxidation and reduction reaction. Polymer **71** gave an O_2 production rate of 140 μmol h^{-1} g^{-1} upon loading with 3 wt% RuOx in the presence of $AgNO_3$, which is higher than those of its counterparts prepared under different powers.

3.3 Conjugated polymers for photocatalytic overall water splitting

In comparison with the aforementioned photocatalytic water reduction or water oxidation, stoichiometric splitting of pure water into hydrogen and oxygen is cost-saving because both

photogenerated electrons and holes are utilized without using a sacrificial agent to suppress one of the half-reactions.[8,166–168] Until now, the reports of efficient CPs for photocatalytic overall water splitting remains rare.

In 2016, Wang *et al.* demonstrated that Pt modified g-C_3N_4 was an efficient photocatalyst for overall water splitting and the morphology of g-C_3N_4 significantly affected the catalytic activity.[169] Among the three types of g-C_3N_4, the urea-derived g-C_3N_4 exhibits a 2D nanosheet structure and compact layer-like morphology, which showed better charge mobility as compared to the other two samples made from dicyandiamide and ammonium thiocyanate as the precursor. All three types of pure g-C_3N_4 have no photocatalytic activity in the absence of Pt. After depositing Pt on the three samples, g-C_3N_4 nanosheets exhibited the best activity with H_2 and O_2 evolution rates of 1.2 and 0.6 μmol h^{-1}, respectively (>420 nm). Very recently, Zhang and co-workers prepared 3D g-C_3N_4 with high crystallinity, displayed a larger surface area (130 m^2 g^{-1}) than those of bulk g-C_3N_4 (10.83 m^2 g^{-1}) and g-C_3N_4 nanosheets (93.84 m^2 g^{-1}).[170] Surprisingly, after loading 1 wt% Pt and 3 wt% IrO_2, 3D g-C_3N_4 exhibited H_2 and O_2 generation rates of 101.4 and 49.1 μmol h^{-1} g^{-1}, respectively, which are about 11.8 and 5.1-fold higher than those of bulk g-C_3N_4 and g-C_3N_4 nanosheets. These examples demonstrated the critical role of the cocatalyst and surface morphology control of g-C_3N_4 in photocatalytic overall water splitting performance.

In 2017, Xu and co-workers prepared 1,3-diyne-linked CMPs **72**–**73** by Glaser oxidative coupling of terminal alkynes.[40] TEM measurements revealed that both polymers have sheet-like structures (Fig. 17a and b), which favours the separation and transport of photogenerated excitons to the surface of polymer nanosheets for water redox reactions. The CB/VB levels were determined to be −3.55/−6.5 eV for **72** and −2.9/−5.77 eV for **73**, indicating that both polymers have appropriate electronic band structures for overall water splitting under the given conditions. As a result, both H_2 and O_2 are evolved for **73** with expected 2 : 1 stoichiometry upon light irradiation (Fig. 17c). The HER is 218 μmol h^{-1} g^{-1} for **73**, which is higher than that of **72** (102 μmol h^{-1} g^{-1}). This could be attributed to the lower band gap of **73** (2.85 eV) compared to **72** (2.94 eV). This work demonstrates the great potential of polymer nanosheets as unique photocatalysts for overall water splitting.

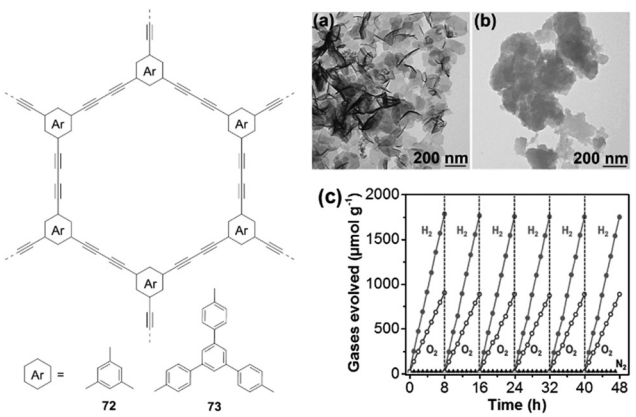

Fig. 17 Chemical structures of polymers **72** and **73**; TEM pictures of (a) **72** and (b) **73** as well as (c) time course of H_2 and O_2 production of polymer **73**. Reprinted with permission from ref. 40. Copyright 2017 Wiley-VCH.

4. Conjugated polymers for photocatalytic CO_2 reduction

4.1 Photocatalytic CO_2 reduction

The massive consumption of fossil fuels has caused the CO_2 levels in the atmosphere to increase over the years, which has raised serious environmental and safety concerns. One of the best solutions to address this challenge is to convert CO_2 into hydrocarbon fuels using solar light as an energy source.[10,11,13,171–174] The technology could create huge economic and environmental benefits by simultaneously reducing the greenhouse effect and solving the energy shortage issue. However, CO_2 is a very stable linear molecule. Compared with that of C–C (336 kJ mol^{-1}), C–H (411 kJ mol^{-1}), and C–O (327 kJ mol^{-1}), an energy input of ~750 kJ mol^{-1} is required for the cleavage of a C═O bond,[13] which makes the conversion of CO_2 very challenging. In a typical CO_2 photoreduction process, water is required to provide a hydrogen source to achieve CO_2 transformation. The adsorption and activation of CO_2 by photocatalysts was a prerequisite for this transformation. Importantly, the redox potential alignment of the photocatalyst must be sufficient to drive the reaction. The potentials of CO_2 reduction in water are given in Table 2 (pH = 7).[13] Reduction of CO_2 by one-electron transfer to generate $CO_2^{\bullet-}$ is not feasible due to the large negative reduction potential of −1.85 V (*vs.* NHE). However, relatively lower reduction potentials of −0.61, −0.53, −0.48, −0.38 and −0.24 V are required for the generation of HCOOH, CO, HCHO, CH_3OH, and CH_4, respectively. A favourable potential of −0.42 V is required for water reduction to generate H_2, which is a strong competitive reaction during the CO_2 photoreduction process. Therefore, depending on the reaction pathways taken and the number of photogenerated electrons transferred, many different products are possible for CO_2 photoreduction, making it difficult to achieve both good selectivity and high efficiency by a given photocatalyst. The selectivity (Φ) of the reacted electrons for CO_2 reduction could be calculated using the following equation:

$$\Phi(\%) = \frac{\text{Number of reacted electrons for } CO_2 \text{ reduction}}{\text{Number of reacted electrons in all reduction reactions}} \times 100\%$$

Table 2 The reduction potentials *versus* NHE for CO_2 reduction in aqueous media (pH = 7). Adapted with permission from ref. 13. Copyright 2018 Wiley-VCH

Entry	Reaction	E_0 *vs.* NHE (V)
1	$CO_2 + e^- \rightarrow CO_2^{\bullet-}$	−1.85
2	$CO_2 + 2H^+ + 2e^- \rightarrow HCOOH$	−0.61
3	$CO_2 + 2H^+ + 2e^- \rightarrow CO + H_2O$	−0.53
4	$CO_2 + 2H^+ + 4e^- \rightarrow HCHO + H_2O$	−0.48
5	$CO_2 + 6H^+ + 6e^- \rightarrow CH_3OH + 6H_2O$	−0.38
6	$CO_2 + 8H^+ + 8e^- \rightarrow CH_4 + 2H_2O$	−0.24
7	$2H^+ + 2e^- \rightarrow H_2$	−0.42

Heterogeneous CO_2 photoreduction over porous polymers was performed in either liquid–solid or gas–solid systems. In a liquid–solid system, the polymer particles were suspended in the CO_2-saturated aqueous solution. Under light irradiation, the CO_2 reduction reactions take place at the interface of the liquid–solid phase. Organic sacrificial agents such as triethanolamine are needed to consume undesirable holes. In contrast, CO_2 photoreduction in a gas–solid system is much simpler and only water vapour is used as the electron donor. In this case, photocatalysts were uniformly dispersed at the bottom of the reactor. Water vapour and CO_2 were chemisorbed and activated by a porous polymer followed by the reduction of CO_2 under light irradiation.

Most of the photocatalysts for CO_2 reduction are inorganic compounds such as metal oxides or sulphides, *e.g.* TiO_2, CdS, $BiVO_4$, *etc.*[163,171] Organic polymers have been relatively less explored so far. For the development of highly active porous CPs for CO_2 photoreduction, some critical factors such as band gaps, surface area, CO_2 absorption, energy level alignments and photogenerated charge separation of the polymers are needed to be taken into account for pursuing good photocatalytic activities and selectivity. In addition, the external environment and operating conditions, such as catalyst quantity, solution pH, CO_2 pressure, temperature, *etc.* will also likely influence the activity and selectivity of the reactions. For the liquid–solid system, the very low CO_2 solubility in the reaction media is one major hurdle to achieve high CO_2 reduction efficiency for the photocatalyst. To address this issue to some extent, Liu *et al.* used ionic liquids to capture more CO_2 from air for the reduction reaction.[175] It was estimated that ~33 mg of CO_2 was captured by 1 g of ionic liquid. By introducing different functional monomers, the CBs of polymers **74–78** (Fig. 18) are varied from −0.78 and −1.52 eV, indicating sufficient driving force for the reduction of CO_2 to CO. The CO production rate follows the order: **78** > **76** > **77** > **75** > **74**. The result was largely determined by the CB values of the CPs. Polymer **78** shows the highest CO production rate of 47.37 μmol h^{-1} g^{-1} with an excellent selectivity of up to 98.3%, which is attributed to its most negative CB value and the largest photocurrent.

g-C_3N_4 also has a favourable CB position to drive the reduction of CO_2 into hydrocarbons, which makes them potential candidates in this field.[30,176] For example, Huang *et al.* reported that fluorine doped boron carbon nitride (BCN–F) could efficiently catalyse the reduction of CO_2 into CO in the CH_3CN/H_2O/TEOA mixture, which gave 3-times higher CO generation rate (7.75 μmol h^{-1}) than pristine BCN.[177] Wang *et al.* synthesized barbituric acid modified g-C_3N_4 nanosheets (CN–BAN) through copolymerization between urea and barbituric acid (BA).[178] With an optimal amount of BA, CN–BAN could produce CO and H_2 with a rate of ~14 μmol h^{-1} and ~3.1 μmol h^{-1}, respectively. In addition, Guo and co-workers prepared g-C_3N_4 nanosheets with nitrogen vacancies (CN–NV) by polymerization of dicyandiamide in the presence of tartaric acid.[179] It was found that the introduction of defects could not only prolong the lifetimes of charge carriers, but also improve the visible light absorption and charge transfer; thereby, CN–NV exhibited

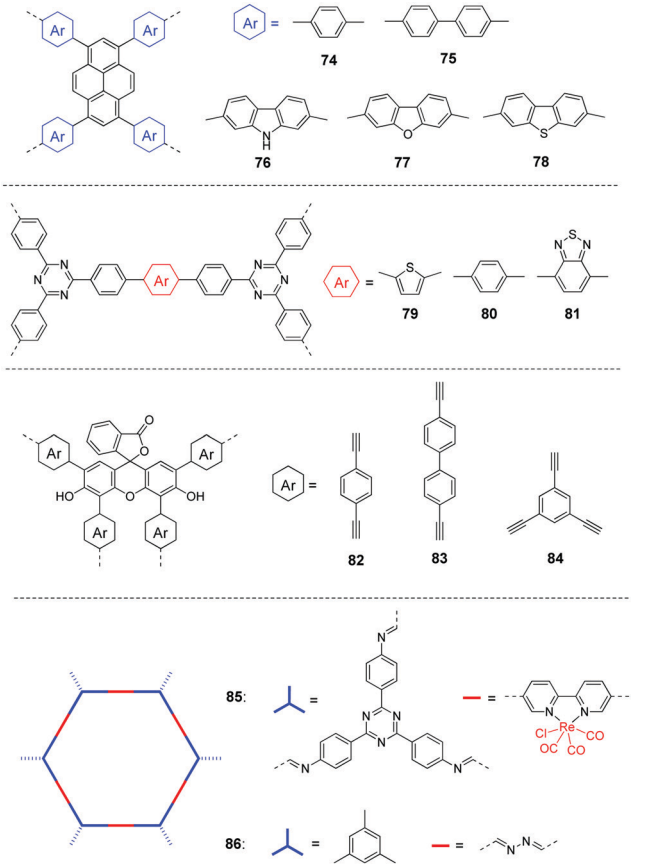

Fig. 18 Chemical structures of polymers **74–86** for photocatalytic CO_2 reduction.

a CO formation rate of 56.9 μmol h^{-1} g^{-1}, which is about 8 times higher than that of pristine g-C_3N_4.

Apart from g-C_3N_4, CTFs with high nitrogen content are expected to have good CO_2-philic ability and thus facilitate the reduction of CO_2. Wang and co-workers developed triazine-based conjugated polymers **79–81**,[180] which showed tunable band gaps of 2.24–2.93 eV due to the D–A interaction between the triazine unit and comonomers. The BET surface areas were 409, 52, and 37 m^2 g^{-1} for **79**, **80**, and **81**, respectively. After loading $CoCl_2$ and dipyridyl as cocatalysts, polymer **81** gave the highest CO generation rate of 18.2 μmol h^{-1} with 81.6% selectivity, which is due to the enhanced charge separation by incorporating electron-withdrawing BT units into the polymer.

Considering the advantages of relatively simple and inexpensive gas–solid systems, Liu *et al.* reported polymers **82–84** by introducing different arylethynylenes.[181] The BET surface areas were 445, 131, and 610 m^2 g^{-1} for **82**, **83**, and **84**, respectively. The highest BET surface area of polymer **84** has thus led to a CO_2 adsorption capacity of 62 mg g^{-1} at 1.0 bar, while lower capacities of 39 and 24 mg g^{-1} were measured for **82** and **83**, respectively. In addition, the band gaps are 2.42–2.53 eV for the three polymers. The combination of electrochemical impedance spectroscopy (EIS) and transient photocurrent response measurements demonstrated that **82** had the best charge transfer

efficiency. Therefore, polymer **82** exhibited the highest CO production rate of 33 μmol g^{-1} h^{-1} with 92% selectivity (Table 3).

COFs have inherent features of crystalline porous structures, which facilitate more efficient charge separation. Thus, this kind of material is used for CO_2 photoreduction. Huang and co-workers developed COF **85**, in which the photoactive COF served as the photosensitizer and Re complex ($Re(bpy)(CO)_3Cl$) was incorporated as a CO_2 reduction catalyst.[182] Transient absorption spectroscopy showed a lifetime of 171 ps for the excited state of **85**, which was much longer than that of the pristine COF, indicating that the incorporation of the Re moiety inhibits charge recombination in **85**. COF **85** could produce ~15 mmol CO/g with 98% selectivity in the TEOA/water mixture after visible light illumination for 22 h.

g-C_3N_4 could also be modified for CO_2 photoreduction in the gas phase. For instance, Yu *et al.* prepared O-doped g-C_3N_4 (CN–O) with a tube-like morphology by a two-step process, which involves thermal exfoliation of the bulk g-C_3N_4 into a nanosheet and curling-condensation of the nanosheet into a nanotube.[183] Compared with bulk g-C_3N_4, the as-prepared hierarchical nanotube exhibited a narrower band gap, higher CO_2 uptake and better charge separation. Therefore, CN–O showed a methanol production rate of 0.88 μmol h^{-1} g^{-1}, which is 5 times larger than that of bulk g-C_3N_4. Wang and co-workers prepared modified g-C_3N_4 with carbon vacancies (CN–CV) by heat treatment of pre-synthesized g-C_3N_4 under an NH_3 atmosphere.[184] This modification improves light absorption and CO_2 adsorption/activation for CN–CV, as compared to pristine g-C_3N_4. Moreover, the charge generation and separation of g-C_3N_4 are also enhanced. As a result, CN–CV displayed a CO production rate of 4.18 μmol h^{-1} g^{-1}, nearly 3.3 times higher than that of pristine g-C_3N_4.

COFs are also efficient in a gas–solid system; azine-linked COFs **45** and **86** were reported for the photoconversion of CO_2 with gaseous H_2O into methanol under visible light.[185] COF **45** showed a higher BET surface area of 1412 m^2 g^{-1}, much higher than **86** (1053 m^2 g^{-1}), which is expected to absorb more CO_2 for the reduction reaction. With a smaller optical gap of 2.57 eV than **86** (2.67 eV) and better photogenerated charge transfer, COF **45** produced 13.7 μmol g^{-1} of CH_3OH after 24 h. The amount is much higher than that of **86** (8.6 μmol g^{-1}) and C_3N_4 (4.8 μmol g^{-1}) under the same conditions.

5. Conjugated polymers for photocatalytic organic transformation

Light-initiated organic transformation is a fascinating tool for the synthesis of many important compounds under mild conditions.[15–17] In recent years, CPs have been intensively studied for organic transformation and different types of photochemical reactions were carried out in high yields with good selectivity under visible light (Fig. 19).[18,19,157–160] As compared to those homogeneous systems for organic transformation, heterogeneous polymer photocatalysts have distinct advantages in terms of structural robustness, non-toxicity, low cost and good recyclability. In general, a photocatalytic organic transformation is initiated by excitation of the polymer photocatalyst to generate electrons

Table 3 Summary of photocatalytic CO_2 reduction using porous CPs under visible light

Polymer	Optical gap (eV)	HOMO/LUMO	S_{BET} (m^2 g^{-1})	Cocatalyst	Sacrificial agent	Main products and highest yield	Selectivity (%)	Ref.
74	2.48	1.70/−0.78 (eV)	27.6	—	TEOA	14.53 (CO)/5.90 (H_2) (μmol h^{-1} g^{-1})	71.1	175[a]
75	2.17	1.26/−0.91 (eV)	14.0	—	TEOA	27.45 (CO)/1.16 (H_2) (μmol h^{-1} g^{-1})	95.9	175[a]
76	2.86	1.40/−1.46 (eV)	442.8	—	TEOA	41.44 (CO)/1.20 (H_2) (μmol h^{-1} g^{-1})	97.2	175[a]
77	2.76	1.61/−1.15 (eV)	4.5	—	TEOA	31.76 (CO)/1.16 (H_2) (μmol h^{-1} g^{-1})	96.5	175[a]
78	2.66	1.14/−1.52 (eV)	23.9	—	TEOA	47.37 (CO)/0.81 (H_2) (μmol h^{-1} g^{-1})	98.3	175[a]
79	2.24	1.55/−0.69 (V *vs.* NHE)	52	$CoCl_2$ and dipyridyl	TEOA	4 (CO)/2 (H_2) (μmol h^{-1})	66.7	180[b]
80	2.93	1.66/−0.77 (V *vs.* NHE)	409	$CoCl_2$ and dipyridyl	TEOA	10 (CO)/3 (H_2) (μmol h^{-1})	76.9	180[b]
81	2.43	2.08/−0.85 (V *vs.* NHE)	37	$CoCl_2$ and dipyridyl	TEOA	18.2 (CO)/4.1 (H_2) (μmol h^{-1})	81.6	180[b]
82	2.45	1.50/−0.95 (eV)	445	—	—	33 (CO)/2.8 (H_2) (μmol h^{-1})	92	181[c]
83	2.53	1.57/−0.96 (eV)	131	—	—	~26 (CO)/~3.0 (H_2) (μmol h^{-1})	90	181[c]
84	2.42	1.48/−0.94 (eV)	610	—	—	~12 (CO)/~29 (H_2) (μmol h^{-1})	29	181[c]
85	—	—	—	—	TEOA	~900 (CO)/~18 (H_2) (μmol h^{-1} g^{-1})	98	182[d]
44	2.57	—	1412	—	—	37 (CH_3OH) (μmol h^{-1} g^{-1})	~100	185[e]
86	2.69	—	1053	—	—	57 (CH_3OH) (μmol h^{-1} g^{-1})	~100	185[e]
BCN–F	2.81	1.93/−0.88 (eV) (V *vs.* NHE)	—	$CoCl_2$ and dipyridyl	TEOA	7.75 (CO) (μmol h^{-1})	~100	177[f]
CN–BAN	—	—	54	$CoCl_2$ and dipyridyl	TEOA	~14 (CO)/~3.1 (H_2) μmol h^{-1}	81.9	178[g]
CN–NV	2.49	1.66/−0.83 (V *vs.* NHE)	29.5	$CoCl_2$ and dipyridyl	TEOA	56.9 (CO)/10.3 (H_2) μmol h^{-1}	84.7	179[h]
CN–O	2.61	1.73/−0.88 (V *vs.* Ag/AgCl)	36	—	—	0.88 (CH_3OH) μmol h^{-1} g^{-1}	100	183[i]
CN–CV	2.79	1.60/−1.19 (V *vs.* NHE)	135.66	—	—	4.18 (CO) μmol h^{-1} g^{-1}	100	184[j]

Reaction conditions: [a] 50 mg of polymer, 10 g of CO_2-saturated ionic liquid, 1 g of TEOA, 220 W xenon lamp (>420 nm). [b] Polymer (15 mg), $CoCl_2$ (1 mmol), dipyridyl (5 mmol), TEOA (1 mL), solvent (5 mL, acetonitrile/water = 4 : 1), CO_2 (1 atm), white light (>420 nm), 30 °C. [c] 10 mg of polymer powder, 300 W Xe lamp (>420 nm), CO_2 and H_2O vapour. [d] 0.9 mg of polymer, 3 mL of CH_3CN, and 0.2 mL of TEOA, 225 W Xe lamp (>420 nm), irradiated for 10 h. [e] 10 mg of polymer, 500 W Xe lamp (800 nm ≥ λ ≥ 420 nm), CO_2 (0.4 MPa) and H_2O vapour, the reactor temperature was kept at 80 °C. [f] 50 mg of catalyst, dipyridine (20 mg), $CoCl_2{\cdot}6H_2O$ (1 mmol), solvent (5 mL, acetonitrile : H_2O = 3 : 2), TEOA (1 mL), CO_2 (1 atm), 300 W xenon lamp (≥420 nm). [g] 30 mg of catalyst, 1 μmol $CoCl_2$, 15 mg of bipyridine, 5 mL of solvent containing 1 mL of TEOA, CO_2 (1 atm), 300 W xenon lamp (>420 nm). [h] 5 mg of catalyst, 4 mL of CH_3CN, 1 mL of TEOA, bipyridine (10 mmol L^{-1}), as well as 25 μL of 20 mmol L^{-1} $CoCl_2$ aqueous solution, 300 W xenon lamp (>400 nm). [i] 50 mg of sample, CO_2 and H_2O vapour, 300 W xenon lamp (>420 nm). [j] 30 mg of polymer, CO_2 and H_2O vapour, 300 W xenon lamp (≥420 nm).

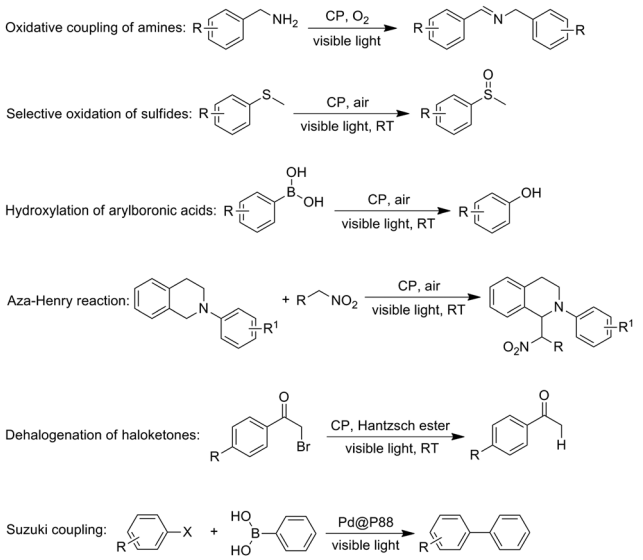

Fig. 19 Typical organic transformation reactions using CPs as the photocatalysts.

and holes, which react with organic substrates to form radical intermediates. These active intermediate species are further converted into final products through rearrangements or reactions with other species at the surface or in bulk solution.[18–20]

5.1 Photocatalytic oxidative coupling of amine

Under light irradiation, polymer semiconductors could generate singlet oxygen ($^1O_2$), which promotes amine oxidative coupling with a broad range of substrates. In 2012, Lin *et al.* synthesized phosphorescent porous polymer **87** with incorporated $[Ru(bpy)_3]^{2+}$ by oxidative homocoupling (Fig. 20).[186] Polymer **87** possesses $[Ru(bpy)_3]^{2+}$ loadings of up to 91 wt%, which not only improves the light absorption but also favours energy migration of the triplet excited states in the polymer network to promote oxidative reactions. Under visible light and at 60 °C, stoichiometric conversions (99%) were achieved for all three substituted benzylamines. Subsequently, Zhang *et al.* developed three CMPs **88–90** by changing the heteroatoms in the benzochalcogenadiazole unit from oxygen to sulfur to selenium.[187] All three polymers can catalyze the oxidative coupling of benzylamine derivatives at room temperature and polymer **89** exhibits the best activity compared to **88** and **90**, which was rationalized by the synergistic effect of the highest BET area, optimized VB and CB band levels and the highest efficiency of electron–hole pair generation. With polymer **89** as the photocatalyst, the reaction illustrates a broad substrate scope with conversions of 5–74%. In parallel, they showed that substitution positions of the benzoxadiazole unit at the centred phenyl unit has a significant impact on the CB/VB of the polymers and their photocatalytic activities. Compared to the other two 3D polymers connecting benzoxadiazole on the 1,2,4- and 1,2,4,5-positions of the phenyl unit, polymer **88** with the 1,3,5-substitution position of the centred phenyl ring demonstrated superior photocatalytic activity.[188] With a high specific surface area of 1137 $m^2\ g^{-1}$ and a broad light absorption in the visible region, the excited polymer **91** could reduce the molecular O_2 to generate superoxide radicals (E_{red} = −0.86 V *vs.* SCE), which can oxidize the primary amine to imine products with 94–98% yields.[189] Directly using natural sunlight, polymer **92** exhibited good conversion ranging from 77 to 99% for oxidative homocoupling of benzylamine, which provided a cost-effective way for large-scale photochemical applications in the future.[190]

5.2 Photocatalytic selective sulfide oxidation

In recent years, significant progress has been made by applying CPPs as photocatalysts for selective sulfide oxidation.[191–193] In 2014, Zhang *et al.* presented the photooxidation of thioanisole using polymer **93** with high porosity.[194] By introducing a BT unit as the strong acceptor into the conjugated backbone, polymer **93** shows a lower band gap of 2.47 eV compared to its counterpart polymer incorporating a carbazole unit. A number of thioanisole derivatives could be photooxidized by polymer **93** with 33–98% conversion and selectivity up to 88–99% after 24 h irradiation of visible light. Upon incorporation of BODIPY dyes into the polymer network, polymer **94** exhibited a bright red emission in the solid state with efficient singlet oxygen generation, which contributed to trigger the oxidation of sulfides with excellent conversion and selectivity.[195] With superior surface area and good activity to reduce O_2 into the superoxide radical, polymer **91** could oxidize thioanisole to the corresponding sulfoxide with excellent selectivity (>93%) and 90–99% yields.[189] Notably, the reactions were completed in a short reaction time of 4.5–12 h, which was strongly influenced by the electron-donating/withdrawing substituents on various substrates.

5.3 Hydroxylation of arylboronic acid

As versatile intermediates for the synthesis of important natural products and pharmaceutical compounds, phenols could be directly synthesized by the hydroxylation of arylboronic acids in air under light illumination. Zhang *et al.* designed polymer **95** using biphenyl as the core and the polymer had a BET area of up to 2065 $m^2\ g^{-1}$.[196] Moreover, polymer **95** exhibited a half wave potential at +1.38 V (*vs.* SEC), indicating its strong oxidation ability. With Et_3N as a sacrificial reductant, this polymer can catalyze the hydroxylation of arylboronic acids bearing various substituents with excellent yields (71–97%). Subsequently, Wang *et al.* reported the conversion of arylboronic acid derivatives to the corresponding phenols using benzoxazole-based COF **103** as the metal-free photocatalyst.[197] Prepared by reversible/irreversible cascade reactions, COF **103** exhibited super stability against light, strong acids and bases. The COF has an optical gap of 2.02 eV with a BET area of up to 1035 $m^2\ g^{-1}$. Under air, polymer **103** displayed 55–99% yields for a range of substrates and the polymer could be recycled for at least 20 catalytic runs.

5.4 Aza-Henry reaction

The aerobic cross dehydrogenative coupling reaction offers a powerful method for the conversion of C–H bonds adjacent to nitrogen atoms into C–C bonds under mild conditions. This reaction plays an increasingly critical role in obtaining natural products and biologically active molecules. Over the

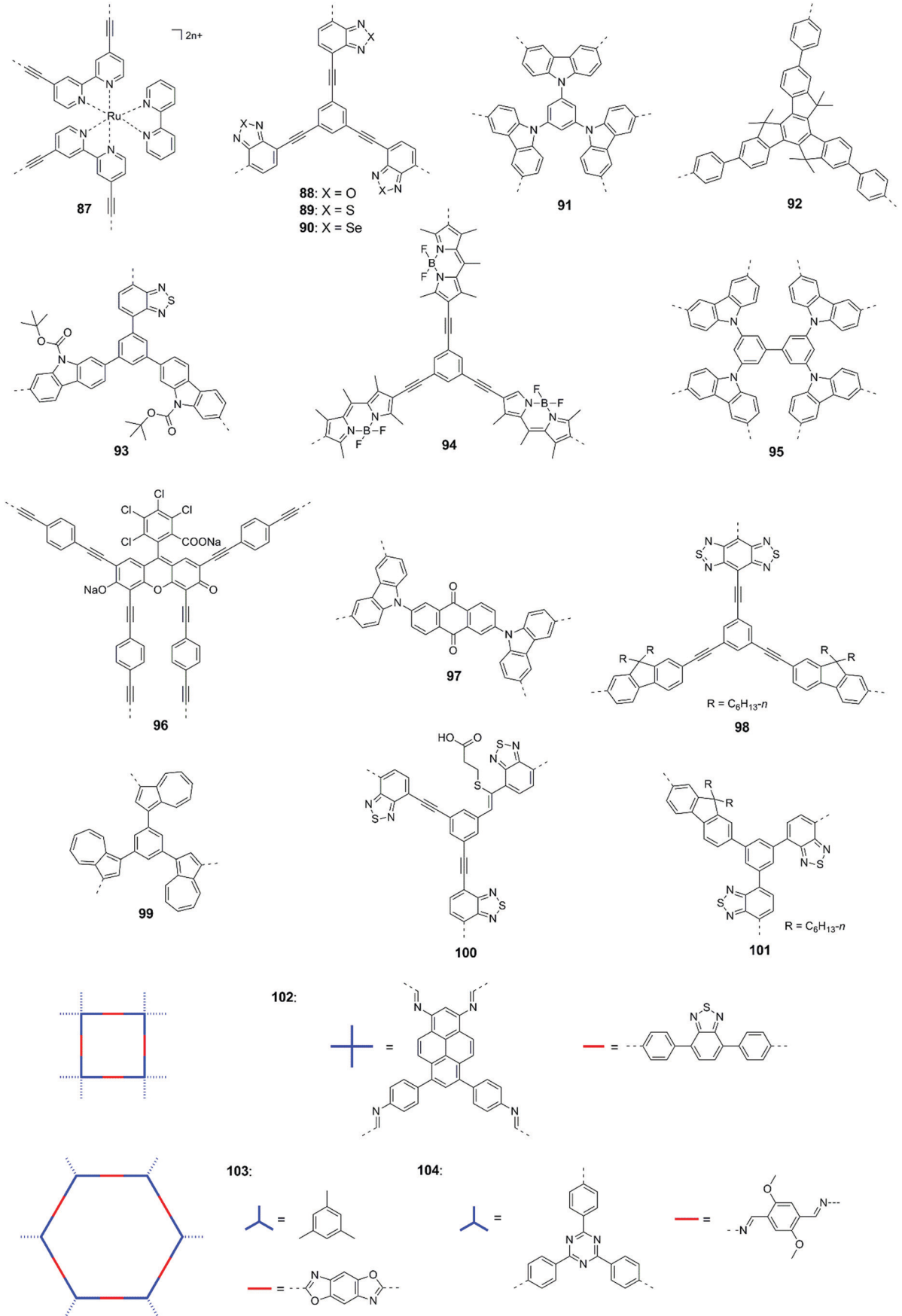

Fig. 20 Typical polymerization methods used to synthesize conjugated polymers for photocatalysis.

last decade, there has been increasing interest in developing CP photocatalysts for this reaction. As a commonly used organic dye, rose bengal was incorporated into polymer **96**, which shows a broad absorption from 350 to 700 nm and a BET surface area of 833 $m^2\ g^{-1}$.[198] 23 substrates were transformed into desirable products with 80–97% isolated yields using a common fluorescent lamp as the light source at room temperature. With good crystallinity and stability, 2D COF **104** exhibited excellent performance for the C–C/C–P coupling reaction with 45–92% yields and a reaction time of 6–11 h without loading any cocatalysts.[199] In this case, the interaction between the donor (2,5-dimethoxybenzene) and acceptor (2,4,6-triphenyl-1,3,5-triazine) in the polymer was expected to improve the photoelectric properties of the resulting COF. Based on the donor–acceptor strategy, they recently synthesized three CMPs by alternating the central core with different electron-deficient units.[200] Compared to the CMPs with incorporated benzene (2.385 eV) and 4,7-diphenyl-2,1,3-benzothiadiazole (2.199 eV), polymer **97** exhibited the smallest optical gap of 1.994 eV. Under visible light irradiation, polymer **97** could catalyse the conversion of 1,2,3,4-tetrahydroisoquinoline derivatives to the desired products with 82–94% yields in 1 h.

5.5 Reductive dehalogenation of haloketones

Besides photo-oxidation reactions, CPs are also very efficient in catalysing some reduction reactions. Photocatalytic reductive dehalogenation of haloketones was one of the most widely investigated reactions. In 2014, Zhang *et al.* reported that polymer **98**, prepared by Sonogashira-coupling in a high internal phase emulsion, exhibited excellent activity for dehalogenation of haloketones with 15–97% yields in 4–5 h at room temperature.[43] The incorporation of benzobisthiadiazole (BBT) unit as a strong electron acceptor into the polymer backbone led to a much lower band gap of 1.5 eV and significantly higher electron paramagnetic resonance (EPR) signals for polymer **98** as compared to its counterpart without the BBT unit. With promising photoredox properties and high porosity, polymer **95** can catalyze the transformation of phenacyl bromide derivatives into acetophenones in 79–98% yields after 24 h light irradiation.[201] Polymer **102** exhibits good crystallinity with a strong diffraction peak at 2.67° and forms irregular block nanocrystals with a size of 60–80 nm.[202] With a BET area of 945 $m^2\ g^{-1}$ and a band gap of 2.08 eV, polymer **102** could catalyse many α-bromoacetophenones to the corresponding acetophenone compounds in 69–88 yields.

5.6 C–C coupling reactions

Cross-coupling reactions, such as Pd(0)-catalyzed Suzuki or Stille coupling reactions, are one of the most important methods for the construction of C–C bonds in organic synthesis.[203,204] In general, these coupling reactions are carried out in homogeneous systems under thermal conditions. However, the Pd(0) catalysts are not stable enough and tend to undergo rapid deactivation during the reaction, which greatly affects the reaction efficiency. Therefore, the synthesis of these targets by stable and robust photocatalysts has attracted increasing attention.[205,206] Zhang *et al.* reported Pd decorated CMP **88** (Pd@P88) for C–C coupling reactions at ambient temperature.[207] TEM images demonstrated that Pd NPs with sizes of 5–10 nm were distributed in the polymer network after treating the polymer with $Pd(OAc)_2$ at 90 °C for 1 h. The Pd content in Pd@P88 was determined to be 3% by ICP measurements. After immobilization with Pd NPs, the band gap of polymer **88** was slightly decreased from 2.43 eV to 2.38 eV. Pd@P88 has a BET surface area of 176 $m^2\ g^{-1}$ and VB/CB of +1.43/−0.95 eV (*vs.* SCE). 75–98% conversion was achieved for the coupling between aryl halides and arylboronic acid with a range of substrates. CPs could also be used for the photocatalytic Stille coupling reaction. Zhang *et al.* disclosed that an azulene-containing CMP **99** could catalyse the Stille coupling reaction between aryl iodides and aryl stannanes under visible light at room temperature.[208] Polymer **99** exhibits a band gap of 2.03 eV with HOMO/LUMO of 1.14/−1.10 V (*vs.* SCE). Notably, only electron-withdrawing-group substituted aryl iodides could be coupled with aryl stannanes due to their lower activated energies than the LUMO of **99** (−1.10 V *vs.* SCE), while electron-donating-group substituted or unsubstituted phenyl iodides are not applicable.

Besides those critical advances in photoredox organic transformations, several new reactions were recently exploited using CPs as the photocatalysts. For instance, polymer **89** was used for photocatalytic C–C double bond cleavage in aqueous media.[209] Various styrene derivatives could be cleaved to afford aldehydes with 27–65% conversion and 92–99% selectivity. Yu and co-workers reported three conjugated microporous polymers for C-3 functionalization of indoles;[210] morphology and oxidation of polymers played an important role in determining the catalytic efficiency.

6. Conjugated polymers for photocatalytic degradation of organic dyes

As one of the most common contaminants in wastewater from textile industries, commercial organic dyes such as methylene blue (MB), rhodamine B (RhB), methyl orange (MO) are chemically stable and could not be removed by microbial processes.[211] Other techniques such as adsorption, ozonation and flocculation have been proven to be insufficient for treatment of these effluents. Photocatalytic degradation of organic dyes into less hazardous compounds offers an attractive method for environmental remediation.[22,23,36,39,212,213] The degradation rate of organic dyes could be facilely monitored using UV-vis absorption spectroscopy.

The degradation process of organic dyes using semiconductors is complicated and the detailed mechanism is not well revealed in the literature. A combination of electron paramagnetic resonance (ESR) analyses and radical species trapping experiments revealed that singlet oxygen ($^1O_2$), superoxide radical ($^{\bullet}O_2^-$), photogenerated hole (h^+), and $HO^{\bullet}$ are the main reactive species in

the process, and the generation of these species could be proposed as follows:

$$e^- + O_2 \rightarrow O_2^{\bullet -} \quad (1)$$

$$O_2^{\bullet -} + H^+ \rightarrow HOO^{\bullet} \quad (2)$$

$$HOO^{\bullet} \rightarrow H_2O_2 + O_2 \quad (3)$$

$$H_2O_2 + O_2^{\bullet -} \rightarrow HO^{\bullet} + O_2 + HO^- \quad (4)$$

$$H_2O_2 + h^+ \rightarrow 2HO^{\bullet} \quad (5)$$

$$H_2O_2 + h\nu \rightarrow 2HO^{\bullet} \quad (6)$$

The photogenerated e^- could react with adsorbed O_2 in the reaction media to generate non-selective $O_2^{\bullet -}$ radicals (eqn (1)) because of the low negative redox potential of $O_2^{\bullet -}/O_2$ (−0.13 eV *vs.* NHE, pH = 7).[36] $O_2^{\bullet -}$ could react with H^+ to give $HO_2^{\bullet}$ (eqn (2)), which could decompose to H_2O_2 and O_2 (eqn (3)). Besides, $HO^{\bullet}$ could be produced by the reaction of H_2O_2 with $O_2^{\bullet -}$ or h^+, as well as its decomposition (eqn (4)–(6)). Moreover, the ROS generation from O_2 by trapping e^- also contributes to inhibit the recombination of electrons and holes. During photocatalysis, these reactive species promote the degradation of organic dyes into CO_2, H_2O and other small molecular products.

Linear CPs with unique nanostructures show great promise for organic dye degradation. Remita *et al.* prepared nanofibers of poly(diphenylbutadiyne) (**105**) by photopolymerization using a soft templating approach (Fig. 21).[214] The nanofibers are a few micrometres long with a diameter of about 19 nm. Without additional sacrificial reagents or cocatalysts, 75% MO were decomposed in water after 240 min irradiation, whereas only 17% MO degradation was achieved by Ag-modified TiO_2. The photocatalytic performance of the nanofibers was almost unchanged even after 15 repeated cycles. Using the same method, they further prepared polymer **106** with vesicle and spindle morphologies, respectively.[215] The spindles are 40 nm thick and the length is several hundred nanometres, while the vesicles are spherical hollow capsules with a diameter of around 1 μm and the thickness of the wall is around 40 nm. A clear shape-dependent photocatalytic activity was demonstrated as shown in Fig. 22a. The nanospindles displayed 100% degradation of MO after 180 min visible light irradiation; by contrast, the vesicles remained totally inactive under identical conditions. Besides, the photocatalytic activity of the polymer **107** nanospindles is much better than that of the polymer **106** nanofibers.

With good photoactivity and excellent water dispersibility, conjugated polyelectrolytes (CPEs) were reported by Zhang and co-workers for organic dye degradation.[216] They prepared polymer **108** by attaching 1-alkyl-3-vinylimidazolium bromide onto the side chains of the poly(benzothiadiazolylfluorene) backbone, which was conducted through a self-initiated radical polymerization process under visible light. With a band gap of 2.11 eV, polymer **108** could almost quantitatively decompose MB and RhB after 70 and 90 min, respectively (Fig. 22b). The good singlet oxygen generation ability of polymer **107** under light excitation is likely responsible for the organic dye photodegradation. In addition, RhB was degraded almost quantitatively in repeated 10 runs, demonstrating excellent stability and reusability of **108**.

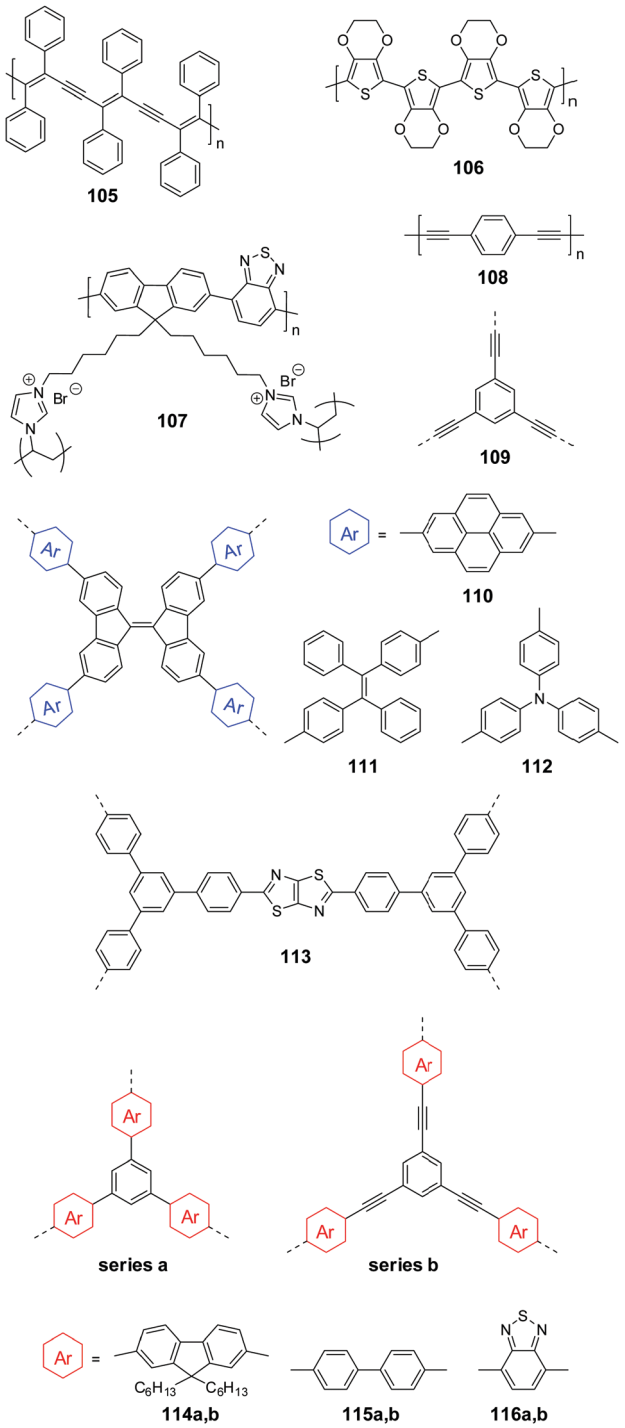

Fig. 21 Representative conjugated polymers for photocatalytic degradation of organic dyes.

Recently, Ouyang and co-workers synthesized three polymers with similar backbone structures and studied the effect of structural variation on their photocatalytic activities.[217] Among them, polymer **109** had a 3D network structure, while the linear polymers **108a** and **108b** were obtained by varying the concentrations of the feeding monomers.

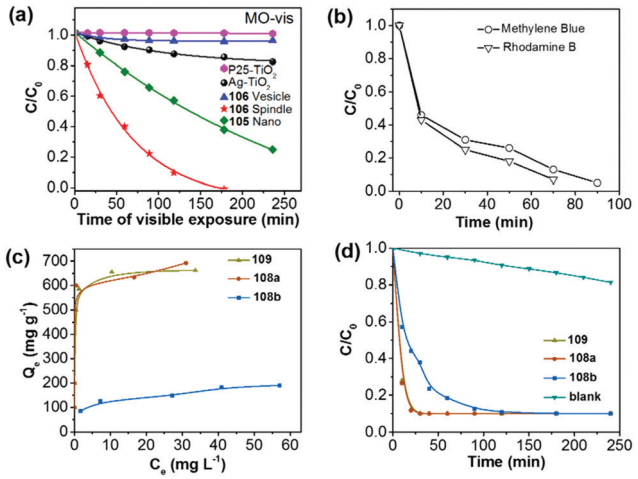

Fig. 22 (a) Comparative photocatalytic degradation of MO of commercial TiO_2, Ag-TiO_2, polymer nanofibers of **105**, vesicles and nanospindles of polymer **106** under visible light (P25-TiO_2 is TiO_2 with a diameter of 25 nm). (b) Photocatalytic degradation of RhB and MB using polymer **107**. (c) The adsorption isotherms of RhB for polymers **108a**, **108b** and **109** at 25 °C. (d) Removal of RhB with polymers **108a**, **108b** and **109** in the supernatant. Reprinted with permission from ref. 215–217. Copyright 2015 Nature Publishing Group, 2015 Wiley-VCH and 2015 Royal Society of Chemistry.

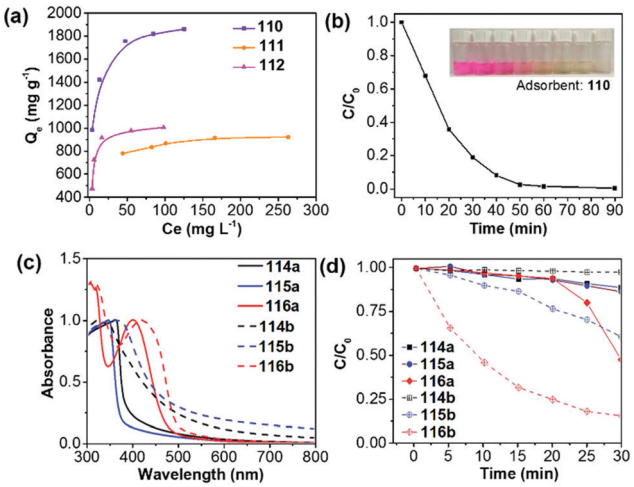

Fig. 23 (a) The adsorption isotherms for RhB on polymers **110–112**. (b) Photocatalytic degradation kinetics of RhB using polymer **110**. (c) UV/vis absorption spectra of NPs of polymers **114–116** in a water dispersion. (d) Photocatalytic degradation of RhB in the presence of NPs of polymers **114–116** in water. Reprinted with permission from ref. 218–220. Copyright 2018 American Chemical Society, 2019 American Chemical Society and 2015 Royal Society of Chemistry.

The BET areas were 1204, 571, 1265 $m^2\ g^{-1}$ for **109a**, **109b** and **109**, respectively. As shown in Fig. 22c, with a high surface area, the adsorption capacities of **110** (661 mg g^{-1}) and **108a** (688 mg g^{-1}) toward RhB were much higher than that of **108b** (189 mg g^{-1}). Polymers **108a** and **108b** exhibited a very close band gap (1.95 eV for **108a** and 1.97 eV for **108b**), which was narrower than that of **109** (2.28 eV). By the synergistic adsorption-photocatalysis, RhB was totally decomposed in 30 min for both **109** and **108a**, while 120 min was needed for 108b to achieve the same performance (Fig. 22d). These results implied that the BET surface area of the polymer played an important role in photocatalytic activity.

The adsorption-photocatalysis synergy was also reported by Chen *et al.*[218] They prepared 9,9′-bifluorenylidene-based porous polymers **110–112** by introducing different comonomers such as pyrene, tetraphenylethene and triphenyl. Polymer **110** with incorporated pyrene units exhibited the lowest band gap of 1.55 eV and the largest BET surface area of 1306 $m^2\ g^{-1}$, while lower surface areas of 777 and 590 $m^2\ g^{-1}$ were determined for **111** and **112**, respectively. All three polymers demonstrated fast uptake of RhB in an aqueous solution. After 45 min, the absorbed percentages of RhB were 97%, 96% and 89% for **110**, **111** and **112**, respectively. As shown in Fig. 23a, polymer **110** exhibited a remarkably high adsorption capacity of 1905 mg g^{-1} of RhB, which is much higher than those of **111** (1024 mg g^{-1}) and **112** (926 mg g^{-1}). As shown in Fig. 23b, more than 81% of RhB was decomposed in the presence of polymer **110** after 30 min visible light irradiation (>450 nm).

Very recently, Jin and co-workers prepared three CMPs with thiazolo[5,4-*d*] thiazole as the linker for photodegradation of organic dyes.[219] Interestingly, the polymers showed nanosheet morphologies and their porous and photophysical properties could be fine-tuned by introducing diphenyl, triphenylbenzene and tetraphenylbenzene. With the highest surface area of 673 $m^2\ g^{-1}$ among the three polymers, polymer **113** could absorb 57% of RhB, while the amount of RhB absorbed by the other two polymers is lower than 15%. Polymer **113** can completely degrade RhB in 30 min and 60 min is needed for the degradation of 80% MO.

Conjugated microporous polymer (CMP) nanoparticles offer unique advantages of high porosity and excellent solution dispersibility compared to bulk catalysts, which is desirable for organic dye photodegradation. Inspired by this, Zhang *et al.* reported the direct preparation of CMP nanoparticles *via* palladium-catalysed polycondensation reactions in a miniemulsion.[220] Interestingly, the difference in the comonomers and linkages has a clear impact on the morphologies and optical properties of the resulting polymers. CMP nanoparticles obtained *via* Sonogashira-coupling are larger than the ones obtained *via* Suzuki-coupling. For BT-containing polymers, polymer **116a** showed a rod-like shape, while polymer **116b** formed nanorings in the reaction media. As shown in Fig. 23c, the introduction of BT into the backbone has led to a narrower band gap of the resulting polymers. Over 80% of RhB was degraded in the presence of **116b** after 25 min, while only about 50% of RhB was decomposed for **116a** (band gap: 1.96 eV) after the same period (Fig. 23d). This result is in accordance with the lowest optical band gap of **116b** (1.76 eV).

7. Summary and outlook

In this Review, we have summarized the recent advances in CPs for various photocatalytic applications, including water splitting, CO_2 reduction, organic transformation and organic dye degradation. Since g-C_3N_4 was first demonstrated for water

splitting under visible light in 2009,[140] CPs have drawn intensive interest and represent a new platform in the field of photocatalysis on account of their inherent advantages of earth-abundant nature, tunable band structure and high stability in the photocatalytic process. We discussed all classes of CPs including g-C_3N_4, linear CPs, porous CPs, water-soluble conjugated polyelectrolytes (CPEs), and organic framework materials (COFs and CTFs) in this review article and presented how polymer design could contribute to different photocatalytic reactions. Structurally, linear CPs consist of alternative conjugated units, while CPPs have 3D porous structures, which are expected to facilitate charge transfer in multiple dimensions. Compared to CPPs and linear CPs, crystalline COFs possess a stacked 2D structure, which is beneficial for photogenerated charge transfer, thus boosting the photocatalytic activity. On the other hand, to date, COFs used for heterogeneous photocatalysis still suffer from limited structural variations. Moreover, a Pt cocatalyst is commonly needed for COFs in photocatalytic H_2 production while CPs prepared by Pd-catalyzed coupling reactions could be directly used without adding any cocatalysts. Besides those noble metal cocatalysts (Pt and Pd), the development of earth-abundant and low-cost cocatalysts has recently attracted attention. For instance, nickel-thiolate cluster was found to be a very efficient H_2 production cocatalyst on a COF photoabsorber.[221] This system demonstrated long-term hydrogen evolution activity with a turnover number of up to 103 and the maximum HER reached 941 μmol h^{-1} g^{-1} in the TEOA/H_2O mixture. To improve the water-wettability of the polymers, a family of polymer photocatalysts enriched with CPEs with conjugated backbones and charged side-chains have also been developed, which offered new potential to this field.

The molecular design has undoubtedly played a vital role in achieving the preferred properties of the resulting polymers, such as strong and wide visible light absorption, appropriate band structure, high efficiency of charge separation and transport, as well as good wettability and surface reaction efficiency. These synergy improvements in principle could result in remarkably enhanced catalytic activity. Among the reported strategies, elemental and molecular doping and the introduction of structural defects into the skeleton of g-C_3N_4 have been well developed for achieving enhanced photocatalytic water splitting and CO_2 reduction. In addition, copolymerization of well-designed donors and acceptors has been widely employed to design CPs for photocatalysis, which have brought extended light absorption and improved charge mobility of polymers. The statistical copolymerization for the synthesis of CPPs offered additional opportunity to adjust the band gaps and porosity of polymers.

Despite the great progress made so far, the investigations in this field are in its infancy. The reported CPs suffer from low photocatalytic efficiency, which are far from the practical requirements. Many issues need to be resolved which may include the following:

(1) The development of photocatalytic H_2 production using CPs has evolved rapidly in the past few years. A recorded H_2 generation rate of 60.6 mmol h^{-1} g^{-1} has been achieved, which is very competitive to inorganic counterparts. It is highly expected that more exciting performance could be achieved in the future by designing new polymers, and the combination of computation and experiment appears to be a promising approach for high-throughput screening of polymer libraries. In a very recent report, Cooper and co-workers computationally studied photocatalytic H_2 production using 6354 potential alternating co-polymers, among which more than 170 co-polymers have been synthesized and examined for their H_2 evolution activities.[222] This work well explored the structure–property-performance relationships of candidate co-polymers and successfully discovered new polymers with HERs greater than 6 mmol h^{-1} g^{-1}. Apart from photocatalytic water reduction or oxidation, photocatalytic overall water splitting has been reported by conjugated microporous polymer nanosheets.[40] However, the fundamentals of the photocatalytic process and structure–activity relationship of the polymer are not well understood. Besides, loading metals as cocatalyst could considerably increase the photocatalytic H_2 production activity, but knowledge about the interaction mechanism between the polymer and metal is still not clear.

(2) Until now, relatively few CPs were exploited for photocatalytic CO_2 reduction and most of them suffer from low activities. Likewise, knowledge about reaction pathways and fundamental enhancements for CO_2 reduction is scarce. In order to increase the catalytic performance of the reaction, more work is in urgent demand to optimize the photoactivity and porosity of polymers.

(3) The use of CPs as heterogeneous photocatalysts is rapidly expanding the toolbox of chemical transformations. They have demonstrated good catalytic activities and recyclability for a variety of photochemical reactions. In particular, some reactions were performed directly under natural sunlight. However, the applied reaction types and substrate scope are still limited as compared to those of traditional transition-metal complexes. It is highly desirable to explore new organic molecule transformations, such as more challenging C-heteroatom or C–C functionalization, for heterogeneous polymer photocatalysts.

(4) Photodegradation of organic dyes using CPs presented an effective technology for environmental remediation. Interestingly, nanostructured CPs with good water dispersion have demonstrated excellent degradation ability. Another important finding is that CPPs could decompose organic dyes very efficiently by the adsorption-photocatalysis synergy. In order to achieve better catalytic activity, advanced research should be devoted to optimize the photophysical properties of conjugated polymers to improve the reactive species generation efficiency.

As CPs have the inherent advantages of diverse molecular structures and readily tunable physicochemical properties, there are unlimited opportunities and challenges in developing high-efficiency CPs for various photocatalytic applications. We expect that this review will be a good reference for the next decade of research in this exciting field. With more advances in polymer chemistry and materials science, it is anticipated that critical innovations in photocatalytic technology using CPs could play an increasingly important role in practical applications.

Conflicts of interest

There are no conflicts of interest to declare.

Acknowledgements

This work was supported by the Singapore National Research Foundation (grant no. R279-000-444-281 and R279-000-483-281) and the National University of Singapore (grant no. R279-000-482-133).

References

1 J. Barber, *Chem. Soc. Rev.*, 2009, **38**, 185–196.
2 A. J. Carrillo, J. González-Aguilar, M. Romero and J. M. Coronado, *Chem. Rev.*, 2019, **119**, 4777–4816.
3 X. Chen, S. Shen, L. Guo and S. S. Mao, *Chem. Rev.*, 2010, **110**, 6503–6570.
4 T. Hisatomi, J. Kubota and K. Domen, *Chem. Soc. Rev.*, 2014, **43**, 7520–7535.
5 T. Wang and J. Gong, *Angew. Chem., Int. Ed.*, 2015, **54**, 10718–10732.
6 J. Willkomm, K. L. Orchard, A. Reynal, E. Pastor, J. R. Durrant and E. Reisner, *Chem. Soc. Rev.*, 2016, **45**, 9–23.
7 Y. Wang, H. Suzuki, J. Xie, O. Tomita, D. J. Martin, M. Higashi, D. Kong, R. Abe and J. Tang, *Chem. Rev.*, 2018, **118**, 5201–5241.
8 Z. Wang, C. Li and K. Domen, *Chem. Soc. Rev.*, 2019, **48**, 2109–2125.
9 T. Hisatomi and K. Domen, *Nat. Catal.*, 2019, **2**, 387–399.
10 S. N. Habisreutinger, L. Schmidt-Mende and J. K. Stolarczyk, *Angew. Chem., Int. Ed.*, 2013, **52**, 7372–7408.
11 X. Liu, S. Inagaki and J. Gong, *Angew. Chem., Int. Ed.*, 2016, **55**, 14924–14950.
12 R. Shi, G. I. N. Waterhouse and T. Zhang, *Sol. RRL*, 2017, **1**, 1700126.
13 Z. Sun, N. Talreja, H. Tao, J. Texter, M. Muhler, J. Strunk and J. Chen, *Angew. Chem., Int. Ed.*, 2018, **57**, 7610–7627.
14 C. Wang, Z. Sun, Y. Zheng and Y. H. Hu, *J. Mater. Chem. A*, 2019, **7**, 865–887.
15 L. Shi and W. Xia, *Chem. Soc. Rev.*, 2012, **41**, 7687–7697.
16 J. W. Beatty and C. R. Stephenson, *Acc. Chem. Res.*, 2015, **48**, 1474–1484.
17 I. Ghosh, L. Marzo, A. Das, R. Shaikh and B. König, *Acc. Chem. Res.*, 2016, **49**, 1566–1577.
18 A. Savateev, I. Ghosh, B. König and M. Antonietti, *Angew. Chem., Int. Ed.*, 2018, **57**, 15936–15947.
19 R. Li, J. Byun, W. Huang, C. Ayed, L. Wang and K. A. I. Zhang, *ACS Catal.*, 2018, **8**, 4735–4750.
20 A. Savateev and M. Antonietti, *ACS Catal.*, 2018, **8**, 9790–9808.
21 U. G. Akpan and B. H. Hameed, *J. Hazard. Mater.*, 2009, **170**, 520–529.
22 L. G. Devi and R. Kavitha, *Appl. Catal., B*, 2013, **140–141**, 559–587.
23 C.-C. Wang, J.-R. Li, X.-L. Lv, Y.-Q. Zhang and G. Guo, *Energy Environ. Sci.*, 2014, **7**, 2831–2867.
24 L. Nie and Q. Zhang, *Inorg. Chem. Front.*, 2017, **4**, 1953–1962.
25 L. Bucher, N. Desbois, P. D. Harvey, G. D. Sharma and C. P. Gros, *Sol. RRL*, 2017, **1**, 1700127.
26 S. Y. Tee, K. Y. Win, W. S. Teo, L.-D. Koh, S. Liu, C. P. Teng and M.-Y. Han, *Adv. Sci.*, 2017, **4**, 1600337.
27 X. Wang, S. Blechert and M. Antonietti, *ACS Catal.*, 2012, **2**, 1596–1606.
28 Y. Zheng, L. Lin, B. Wang and X. Wang, *Angew. Chem., Int. Ed.*, 2015, **54**, 12868–12884.
29 W.-J. Ong, L.-L. Tan, Y. H. Ng, S.-T. Yong and S.-P. Chai, *Chem. Rev.*, 2016, **116**, 7159–7329.
30 J. Fu, J. Yu, C. Jiang and B. Cheng, *Adv. Energy Mater.*, 2018, **8**, 1701503.
31 Y. Zheng, J. Liu, J. Liang, M. Jaroniec and S. Z. Qiao, *Energy Environ. Sci.*, 2012, **5**, 6717–6731.
32 J. Zhang, Y. Chen and X. Wang, *Energy Environ. Sci.*, 2015, **8**, 3092–3108.
33 V. S. Vyas, V. W.-h. Lau and B. V. Lotsch, *Chem. Mater.*, 2016, **28**, 5191–5204.
34 G. Zhang, Z. A. Lan and X. Wang, *Angew. Chem., Int. Ed.*, 2016, **55**, 15712–15727.
35 L. Lin, Z. Yu and X. Wang, *Angew. Chem., Int. Ed.*, 2019, **58**, 6164–6175.
36 C. Chen, W. Ma and J. Zhao, *Chem. Soc. Rev.*, 2010, **39**, 4206–4219.
37 M. Marszewski, S. Cao, J. Yu and M. Jaroniec, *Mater. Horiz.*, 2015, **2**, 261–278.
38 J. L. White, M. F. Baruch, J. E. Pander III, Y. Hu, I. C. Fortmeyer, J. E. Park, T. Zhang, K. Liao, J. Gu, Y. Yan, T. W. Shaw, E. Abelev and A. B. Bocarsly, *Chem. Rev.*, 2015, **115**, 12888–12935.
39 L. V. Bora and R. K. Mewada, *Renewable Sustainable Energy Rev.*, 2017, **76**, 1393–1421.
40 L. Wang, Y. Wan, Y. Ding, S. Wu, Y. Zhang, X. Zhang, G. Zhang, Y. Xiong, X. Wu, J. Yang and H. Xu, *Adv. Mater.*, 2017, **29**, 1702428.
41 L. Wang, Y. Wan, Y. Ding, Y. Niu, Y. Xiong, X. Wu and H. Xu, *Nanoscale*, 2017, **9**, 4090–4096.
42 L. Wang, X. Zheng, L. Chen, Y. Xiong and H. Xu, *Angew. Chem., Int. Ed.*, 2018, **57**, 3454–3458.
43 Z. J. Wang, S. Ghasimi, K. Landfester and K. A. I. Zhang, *J. Mater. Chem. A*, 2014, **2**, 18720–18724.
44 Z. J. Wang, S. Ghasimi, K. Landfester and K. A. I. Zhang, *Chem. Commun.*, 2014, **50**, 8177–8180.
45 B. C. Ma, S. Ghasimi, K. Landfester, F. Vilela and K. A. I. Zhang, *J. Mater. Chem. A*, 2015, **3**, 16064–16071.
46 Y.-J. Cheng, S.-H. Yang and C.-S. Hsu, *Chem. Rev.*, 2009, **109**, 5868–5923.
47 X. Feng, X. Ding and D. Jiang, *Chem. Soc. Rev.*, 2012, **41**, 6010–6022.
48 C. Zhu, L. Liu, Q. Yang, F. Lv and S. Wang, *Chem. Rev.*, 2012, **112**, 4687–4735.
49 S.-Y. Ding and W. Wang, *Chem. Soc. Rev.*, 2013, **42**, 548–568.
50 Y. Xu, S. Jin, H. Xu, A. Nagai and D. Jiang, *Chem. Soc. Rev.*, 2013, **42**, 8012–8031.
51 J. L. Segura, M. J. Mancheno and F. Zamora, *Chem. Soc. Rev.*, 2016, **45**, 5635–5671.

52 J.-R. Pouliot, F. Grenier, J. T. Blaskovits, S. Beaupré and M. Leclerc, *Chem. Rev.*, 2016, **116**, 14225–14274.
53 M. Liu, L. Guo, S. Jin and B. Tan, *J. Mater. Chem. A*, 2019, **7**, 5153–5172.
54 M. Leclerc and J.-F. Morin, *Design and synthesis of conjugated polymers*, John Wiley & Sons, 2010.
55 Y. Chujo, *Conjugated polymer synthesis: methods and reactions*, John Wiley & Sons, 2011.
56 M. Karayilan, W. P. Brezinski, K. E. Clary, D. L. Lichtenberger, R. S. Glass and J. Pyun, *Angew. Chem., Int. Ed.*, 2019, **58**, 7537–7550.
57 Y. Ma, X. Wang, Y. Jia, X. Chen, H. Han and C. Li, *Chem. Rev.*, 2014, **114**, 9987–10043.
58 S. Cao and J. Yu, *J. Phys. Chem. Lett.*, 2014, **5**, 2101–2107.
59 L.-Z. Wu, B. Chen, Z.-J. Li and C.-H. Tung, *Acc. Chem. Res.*, 2014, **47**, 2177–2185.
60 S. Kaufhold, L. Petermann, R. Staehle and S. Rau, *Coord. Chem. Rev.*, 2015, **304**, 73–87.
61 X. Zhang, T. Peng and S. Song, *J. Mater. Chem. A*, 2016, **4**, 2365–2402.
62 M. Wen, K. Mori, Y. Kuwahara, T. An and H. Yamashita, *Appl. Catal., B*, 2017, **218**, 555–569.
63 Y. Huang and B. Zhang, *Angew. Chem., Int. Ed.*, 2017, **56**, 14804–14806.
64 Y.-J. Yuan, D. Chen, Z.-T. Yu and Z.-G. Zou, *J. Mater. Chem. A*, 2018, **6**, 11606–11630.
65 M. G. Schwab, M. Hamburger, X. Feng, J. Shu, H. W. Spiess, X. Wang, M. Antonietti and K. Müllen, *Chem. Commun.*, 2010, **46**, 8932–8934.
66 S. Yanagida, A. Kabumoto, K. Mizumoto, C. Pac and K. Yoshino, *J. Chem. Soc., Chem. Commun.*, 1985, **8**, 474–475.
67 T. Shibata, A. Kabumoto, T. Shiragami, O. Ishitani, C. Pac and S. Yanagida, *J. Phys. Chem.*, 1990, **94**, 2068–2076.
68 S. Matsuoka, T. Kohzuki, A. Nakamura, C. Pac and S. Yanagida, *J. Chem. Soc., Chem. Commun.*, 1991, **8**, 580–581.
69 S. Matsuoka, H. Fujii, T. Yamada, C. Pac, A. Ishida, S. Takamuku, M. Kusaba, N. Nakashima and S. Yanagida, *J. Phys. Chem.*, 1991, **95**, 5802–5808.
70 R. S. Sprick, B. Bonillo, R. Clowes, P. Guiglion, N. J. Brownbill, B. J. Slater, F. Blanc, M. A. Zwijnenburg, D. J. Adams and A. I. Cooper, *Angew. Chem., Int. Ed.*, 2018, **57**, 2520.
71 X.-H. Zhang, X.-P. Wang, J. Xiao, S.-Y. Wang, D.-K. Huang, X. Ding, Y.-G. Xiang and H. Chen, *J. Catal.*, 2017, **350**, 64–71.
72 M. Sachs, R. S. Sprick, D. Pearce, S. J. Hillman, A. Monti, A. A. Y. Guilbert, N. J. Brownbill, S. Dimitrov, X. Shi, F. Blanc, M. A. Zwijnenburg, J. Nelson, J. R. Durrant and A. I. Cooper, *Nat. Commun.*, 2018, **9**, 4968.
73 C. M. Aitchison, R. S. Sprick and A. I. Cooper, *J. Mater. Chem. A*, 2019, **7**, 2490–2496.
74 C. Dai, S. Xu, W. Liu, X. Gong, M. Panahandeh-Fard, Z. Liu, D. Zhang, C. Xue, K. P. Loh and B. Liu, *Small*, 2018, **14**, 1801839.
75 Z.-A. Lan, G. Zhang, X. Chen, Y. Zhang, K. A. I. Zhang and X. Wang, *Angew. Chem., Int. Ed.*, 2019, **58**, 10236–10240.
76 R. S. Sprick, C. M. Aitchison, E. Berardo, L. Turcani, L. Wilbraham, B. M. Alston, K. E. Jelfs, M. A. Zwijnenburg and A. I. Cooper, *J. Mater. Chem. A*, 2018, **6**, 11994–12003.
77 R. S. Sprick, L. Wilbraham, Y. Bai, P. Guiglion, A. Monti, R. Clowes, A. I. Cooper and M. A. Zwijnenburg, *Chem. Mater.*, 2018, **30**, 5733–5742.
78 J. Pecher and S. Mecking, *Chem. Rev.*, 2010, **110**, 6260–6279.
79 K. Li and B. Liu, *J. Mater. Chem.*, 2012, **22**, 1257–1264.
80 L. Feng, C. Zhu, H. Yuan, L. Liu, F. Lv and S. Wang, *Chem. Soc. Rev.*, 2013, **42**, 6620–6633.
81 S. Kundu and A. Patra, *Chem. Rev.*, 2016, **117**, 712–757.
82 L. Wang, R. Fernández-Terán, L. Zhang, D. L. Fernandes, L. Tian, H. Chen and H. Tian, *Angew. Chem., Int. Ed.*, 2016, **55**, 12306–12310.
83 P. B. Pati, G. Damas, L. Tian, D. L. Fernandes, L. Zhang, I. B. Pehlivan, T. Edvinsson, C. M. Araujo and H. Tian, *Energy Environ. Sci.*, 2017, **10**, 1372–1376.
84 P.-J. Tseng, C.-L. Chang, Y.-H. Chan, L.-Y. Ting, P.-Y. Chen, C.-H. Liao, M.-L. Tsai and H.-H. Chou, *ACS Catal.*, 2018, **8**, 7766–7772.
85 C. V. Hoven, A. Garcia, G. C. Bazan and T. Q. Nguyen, *Adv. Mater.*, 2008, **20**, 3793–3810.
86 H. Jiang, P. Taranekar, J. R. Reynolds and K. S. Schanze, *Angew. Chem., Int. Ed.*, 2009, **48**, 4300–4316.
87 A. Duarte, K.-Y. Pu, B. Liu and G. C. Bazan, *Chem. Mater.*, 2010, **23**, 501–515.
88 Q. Cui and G. C. Bazan, *Acc. Chem. Res.*, 2017, **51**, 202–211.
89 C. Dai, M. Panahandeh-Fard, X. Gong, C. Xue and B. Liu, *Sol. RRL*, 2019, **3**, 1800255.
90 Z. Hu, Z. Wang, X. Zhang, H. Tang, X. Liu, F. Huang and Y. Cao, *iScience*, 2019, **13**, 33–42.
91 D. J. Woods, R. S. Sprick, C. L. Smith, A. J. Cowan and A. I. Cooper, *Adv. Energy Mater.*, 2017, **7**, 1700479.
92 A. I. Cooper, *Adv. Mater.*, 2009, **21**, 1291–1295.
93 R. Dawson, A. I. Cooper and D. J. Adams, *Prog. Polym. Sci.*, 2012, **37**, 530–563.
94 J. Zhu, C. Yang, C. Lu, F. Zhang, Z. Yuan and X. Zhuang, *Acc. Chem. Res.*, 2018, **51**, 3191–3202.
95 F. Vilela, K. Zhang and M. Antonietti, *Energy Environ. Sci.*, 2012, **5**, 7819–7832.
96 R. S. Sprick, J.-X. Jiang, B. Bonillo, S. Ren, T. Ratvijitvech, P. Guiglion, M. A. Zwijnenburg, D. J. Adams and A. I. Cooper, *J. Am. Chem. Soc.*, 2015, **137**, 3265–3270.
97 Y. Xu, N. Mao, C. Zhang, X. Wang, J. Zeng, Y. Chen, F. Wang and J.-X. Jiang, *Appl. Catal., B*, 2018, **228**, 1–9.
98 Y. Liu, Z. Liao, X. Ma and Z. Xiang, *ACS Appl. Mater. Interfaces*, 2018, **10**, 30698–30705.
99 Z.-A. Lan, W. Ren, X. Chen, Y. Zhang and X. Wang, *Appl. Catal., B*, 2019, **245**, 596–603.
100 Y. Li, *Acc. Chem. Res.*, 2012, **45**, 723–733.
101 H. Zhou, L. Yang and W. You, *Macromolecules*, 2012, **45**, 607–632.
102 C. Gao, L. Wang, X. Li and H. Wang, *Polym. Chem.*, 2014, **5**, 5200–5210.
103 H. Yao, L. Ye, H. Zhang, S. Li, S. Zhang and J. Hou, *Chem. Rev.*, 2016, **116**, 7397–7457.

104 C. Liu, K. Wang, X. Gong and A. J. Heeger, *Chem. Soc. Rev.*, 2016, **45**, 4825–4846.
105 L. Li, Z. Cai, Q. Wu, W.-Y. Lo, N. Zhang, L. X. Chen and L. Yu, *J. Am. Chem. Soc.*, 2016, **138**, 7681–7686.
106 L. Li, W.-y. Lo, Z. Cai, N. Zhang and L. Yu, *Macromolecules*, 2016, **49**, 6903–6909.
107 C. Yang, B. C. Ma, L. Zhang, S. Lin, S. Ghasimi, K. Landfester, K. A. I. Zhang and X. Wang, *Angew. Chem., Int. Ed.*, 2016, **55**, 9202–9206.
108 Q. Zhang, M. A. Kelly, N. Bauer and W. You, *Acc. Chem. Res.*, 2017, **50**, 2401–2409.
109 W. Zhong, J. Liang, S. Hu, X.-F. Jiang, L. Ying, F. Huang, W. Yang and Y. Cao, *Macromolecules*, 2016, **49**, 5806–5816.
110 Y. Xiang, X. Wang, L. Rao, P. Wang, D. Huang, X. Ding, X. Zhang, S. Wang, H. Chen and Y. Zhu, *ACS Energy Lett.*, 2018, **3**, 2544–2549.
111 C. Cheng, X. Wang, Y. Lin, L. He, J.-X. Jiang, Y. Xu and F. Wang, *Polym. Chem.*, 2018, **9**, 4468–4475.
112 S. Bi, Z. A. Lan, S. Paasch, W. Zhang, Y. He, C. Zhang, F. Liu, D. Wu, X. Zhuang and E. Brunner, *Adv. Funct. Mater.*, 2017, **27**, 1703146.
113 Z. Wang, X. Yang, T. Yang, Y. Zhao, F. Wang, Y. Chen, J. H. Zeng, C. Yan, F. Huang and J.-X. Jiang, *ACS Catal.*, 2018, **8**, 8590–8596.
114 R. S. Sprick, B. Bonillo, M. Sachs, R. Clowes, J. R. Durrant, D. J. Adams and A. I. Cooper, *Chem. Commun.*, 2016, **52**, 10008–10011.
115 R. S. Sprick, Y. Bai, A. A. Guilbert, M. Zbiri, C. M. Aitchison, L. Wilbraham, Y. Yan, D. J. Woods, M. A. Zwijnenburg and A. I. Cooper, *Chem. Mater.*, 2019, **31**, 305–313.
116 Y. Zhao, W. Ma, Y. Xu, C. Zhang, Q. Wang, T. Yang, X. Gao, F. Wang, C. Yan and J.-X. Jiang, *Macromolecules*, 2018, **51**, 9502–9508.
117 G. Zhang, W. Ou, J. Wang, Y. Xu, D. Xu, T. Sun, S. Xiao, M. Wang, H. Li, W. Chen and C. Su, *Appl. Catal., B*, 2019, **245**, 114–121.
118 F. Beuerle and B. Gole, *Angew. Chem., Int. Ed.*, 2018, **57**, 4850–4878.
119 L. Stegbauer, K. Schwinghammer and B. V. Lotsch, *Chem. Sci.*, 2014, **5**, 2789–2793.
120 V. S. Vyas, F. Haase, L. Stegbauer, G. Savasci, F. Podjaski, C. Ochsenfeld and B. V. Lotsch, *Nat. Commun.*, 2015, **6**, 8508.
121 X. Wang, L. Chen, S. Y. Chong, M. A. Little, Y. Wu, W.-H. Zhu, R. Clowes, Y. Yan, M. A. Zwijnenburg and R. S. Sprick, *Nat. Chem.*, 2018, **10**, 1180.
122 P. Pachfule, A. Acharjya, J. r. m. Roeser, T. Langenhahn, M. Schwarze, R. Schomäcker, A. Thomas and J. Schmidt, *J. Am. Chem. Soc.*, 2018, **140**, 1423–1427.
123 J. L. Sheng, H. Dong, X. B. Meng, H. L. Tang, Y. H. Yao, D. Q. Liu, L. L. Bai, F. M. Zhang, J. Z. Wei and X. J. Sun, *ChemCatChem*, 2019, **11**, 2313–2319.
124 E. Jin, Z. Lan, Q. Jiang, K. Geng, G. Li, X. Wang and D. Jiang, *Chem*, 2019, **5**, 1632–1647.
125 A. Thomas, *Angew. Chem., Int. Ed.*, 2010, **49**, 8328–8344.
126 K. Sakaushi and M. Antonietti, *Acc. Chem. Res.*, 2015, **48**, 1591–1600.
127 P. Puthiaraj, Y.-R. Lee, S. Zhang and W.-S. Ahn, *J. Mater. Chem. A*, 2016, **4**, 16288–16311.
128 J. Bi, W. Fang, L. Li, J. Wang, S. Liang, Y. He, M. Liu and L. Wu, *Macromol. Rapid Commun.*, 2015, **36**, 1799–1805.
129 S. Kuecken, A. Acharjya, L. Zhi, M. Schwarze, R. Schomäcker and A. Thomas, *Chem. Commun.*, 2017, **53**, 5854–5857.
130 Z.-A. Lan, Y. Fang, X. Chen and X. Wang, *Chem. Commun.*, 2019, **55**, 7756–7759.
131 W. Huang, Q. He, Y. Hu and Y. Li, *Angew. Chem., Int. Ed.*, 2019, **131**, 1–6.
132 K. Wang, L. M. Yang, X. Wang, L. Guo, G. Cheng, C. Zhang, S. Jin, B. Tan and A. I. Cooper, *Angew. Chem., Int. Ed.*, 2017, **56**, 14149–14153.
133 L. Guo, Y. Niu, H. Xu, Q. Li, S. Razzaque, Q. Huang, S. Jin and B. Tan, *J. Mater. Chem. A*, 2018, **6**, 19775–19781.
134 C. B. Meier, R. S. Sprick, A. Monti, P. Guiglion, J.-S. M. Lee, M. A. Zwijnenburg and A. I. Cooper, *Polymer*, 2017, **126**, 283–290.
135 Y. S. Kochergin, D. Schwarz, A. Acharjya, A. Ichangi, R. Kulkarni, P. Eliášová, J. Vacek, J. Schmidt, A. Thomas and M. J. Bojdys, *Angew. Chem., Int. Ed.*, 2018, **57**, 14188–14192.
136 L. Li, W. Fang, P. Zhang, J. Bi, Y. He, J. Wang and W. Su, *J. Mater. Chem. A*, 2016, **4**, 12402–12406.
137 Z. Cheng, W. Fang, T. Zhao, S. Fang, J. Bi, S. Liang, L. Li, Y. Yu and L. Wu, *ACS Appl. Mater. Interfaces*, 2018, **10**, 41415–41421.
138 M. Liu, Q. Huang, S. Wang, Z. Li, B. Li, S. Jin and B. Tan, *Angew. Chem.*, 2018, **130**, 12144–12148.
139 S. Chu, Y. Wang, Y. Guo, P. Zhou, H. Yu, L. Luo, F. Kong and Z. Zou, *J. Mater. Chem.*, 2012, **22**, 15519–15521.
140 X. Wang, K. Maeda, A. Thomas, K. Takanabe, G. Xin, J. M. Carlsson, K. Domen and M. Antonietti, *Nat. Mater.*, 2009, **8**, 76.
141 A. Naseri, M. Samadi, A. Pourjavadi, A. Z. Moshfegh and S. Ramakrishna, *J. Mater. Chem. A*, 2017, **5**, 23406–23433.
142 Y. Wang, Y. Di, M. Antonietti, H. Li, X. Chen and X. Wang, *Chem. Mater.*, 2010, **22**, 5119–5121.
143 J. Fang, H. Fan, M. Li and C. Long, *J. Mater. Chem. A*, 2015, **3**, 13819–13826.
144 H. Wang, B. Wang, Y. Bian and L. Dai, *ACS Appl. Mater. Interfaces*, 2017, **9**, 21730–21737.
145 J. Zhang, X. Chen, K. Takanabe, K. Maeda, K. Domen, J. D. Epping, X. Fu, M. Antonietti and X. Wang, *Angew. Chem., Int. Ed.*, 2010, **49**, 441–444.
146 M. K. Bhunia, K. Yamauchi and K. Takanabe, *Angew. Chem., Int. Ed.*, 2014, **53**, 11001–11005.
147 X. Fan, L. Zhang, R. Cheng, M. Wang, M. Li, Y. Zhou and J. Shi, *ACS Catal.*, 2015, **5**, 5008–5015.
148 J. Zhang, M. Zhang, S. Lin, X. Fu and X. Wang, *J. Catal.*, 2014, **310**, 24–30.
149 H. Yu, R. Shi, Y. Zhao, T. Bian, Y. Zhao, C. Zhou, G. I. Waterhouse, L. Z. Wu, C. H. Tung and T. Zhang, *Adv. Mater.*, 2017, **29**, 1605148.
150 W. Ren, J. Cheng, H. Ou, C. Huang, M. M. Titirici and X. Wang, *ChemSusChem*, 2019, **12**, 3257–3262.

151 Z. Zhang, J. Long, L. Yang, W. Chen, W. Dai, X. Fu and X. Wang, *Chem. Sci.*, 2011, **2**, 1826–1830.
152 J. Chen, C. L. Dong, D. Zhao, Y. C. Huang, X. Wang, L. Samad, L. Dang, M. Shearer, S. Shen and L. Guo, *Adv. Mater.*, 2017, **29**, 1606198.
153 W. Zhou, T. Jia, H. Shi, D. Yu, W. Hong and X. Chen, *J. Mater. Chem. A*, 2019, **7**, 303–311.
154 S. Zang, G. Zhang, P. Yang, D. Zheng and X. Wang, *Chem. – Eur. J.*, 2019, **25**, 6102–6107.
155 M. Luo, Q. Yang, K. Liu, H. Cao and H. Yan, *Chem. Commun.*, 2019, **55**, 5829–5832.
156 G. Zhou, L.-L. Zheng, D. Wang, Q.-J. Xing, F. Li, P. Ye, X. Xiao, Y. Li and J.-P. Zou, *Chem. Commun.*, 2019, **55**, 4150–4153.
157 J. Yang, D. Wang, H. Han and C. Li, *Acc. Chem. Res.*, 2013, **46**, 1900–1909.
158 J. Ran, J. Zhang, J. Yu, M. Jaroniec and S. Z. Qiao, *Chem. Soc. Rev.*, 2014, **43**, 7787–7812.
159 X. Li, J. Yu, M. Jaroniec and X. Chen, *Chem. Rev.*, 2019, **119**, 3962–4179.
160 J. Kosco and I. McCulloch, *ACS Energy Lett.*, 2018, **3**, 2846–2850.
161 J. Kosco, M. Sachs, R. Godin, M. Kirkus, L. Francas, M. Bidwell, M. Qureshi, D. Anjum, J. R. Durrant and I. McCulloch, *Adv. Energy Mater.*, 2018, **8**, 1802181.
162 K. L. Materna, R. H. Crabtree and G. W. Brudvig, *Chem. Soc. Rev.*, 2017, **46**, 6099–6110.
163 D. Kong, Y. Zheng, M. Kobielusz, Y. Wang, Z. Bai, W. Macyk, X. Wang and J. Tang, *Mater. Today*, 2018, **21**, 897–924.
164 Z. A. Lan, Y. Fang, Y. Zhang and X. Wang, *Angew. Chem., Int. Ed.*, 2018, **57**, 470–474.
165 J. Xie, S. A. Shevlin, Q. Ruan, S. J. Moniz, Y. Liu, X. Liu, Y. Li, C. C. Lau, Z. X. Guo and J. Tang, *Energy Environ. Sci.*, 2018, **11**, 1617–1624.
166 S. Chen, T. Takata and K. Domen, *Nat. Rev. Mater.*, 2017, **2**, 17050.
167 G. Zhang, Z.-A. Lan and X. Wang, *Chem. Sci.*, 2017, **8**, 5261–5274.
168 L. Wang, Y. Zhang, L. Chen, H. Xu and Y. Xiong, *Adv. Mater.*, 2018, **30**, 1801955.
169 G. Zhang, Z.-A. Lan, L. Lin, S. Lin and X. Wang, *Chem. Sci.*, 2016, **7**, 3062–3066.
170 X. Chen, R. Shi, Q. Chen, Z. Zhang, W. Jiang, Y. Zhu and T. Zhang, *Nano Energy*, 2019, **59**, 644–650.
171 A. Dhakshinamoorthy, S. Navalon, A. Corma and H. Garcia, *Energy Environ. Sci.*, 2012, **5**, 9217–9233.
172 J. Mao, K. Li and T. Peng, *Catal. Sci. Technol.*, 2013, **3**, 2481–2498.
173 W. Tu, Y. Zhou and Z. Zou, *Adv. Mater.*, 2014, **26**, 4607–4626.
174 J. Ran, M. Jaroniec and S. Z. Qiao, *Adv. Mater.*, 2018, **30**, 1704649.
175 Y. Chen, G. Ji, S. Guo, B. Yu, Y. Zhao, Y. Wu, H. Zhang, Z. Liu, B. Han and Z. Liu, *Green Chem.*, 2017, **19**, 5777–5781.
176 Y. Fang and X. Wang, *Chem. Commun.*, 2018, **54**, 5674–5687.
177 F. Xing, Q. Liu, M. Song and C. Huang, *ChemCatChem*, 2018, **10**, 5270–5279.
178 J. Qin, S. Wang, H. Ren, Y. Hou and X. Wang, *Appl. Catal., B*, 2015, **179**, 1–8.
179 H. Shi, S. Long, J. Hou, L. Ye, Y. Sun, W. Ni, C. Song, K. Li, G. G. Gurzadyan and X. Guo, *Chem. – Eur. J.*, 2019, **25**, 5028–5035.
180 C. Yang, W. Huang, L. C. da Silva, K. A. I. Zhang and X. Wang, *Chem. – Eur. J.*, 2018, **24**, 17454–17458.
181 X. Yu, Z. Yang, B. Qiu, S. Guo, P. Yang, B. Yu, H. Zhang, Y. Zhao, X. Yang, B. Han and Z. Liu, *Angew. Chem., Int. Ed.*, 2019, **58**, 632–636.
182 S. Yang, W. Hu, X. Zhang, P. He, B. Pattengale, C. Liu, M. Cendejas, I. Hermans, X. Zhang and J. Zhang, *J. Am. Chem. Soc.*, 2018, **140**, 14614–14618.
183 J. Fu, B. Zhu, C. Jiang, B. Cheng, W. You and J. Yu, *Small*, 2017, **13**, 1603938.
184 M. Shen, L. Zhang, M. Wang, J. Tian, X. Jin, L. Guo, L. Wang and J. Shi, *J. Mater. Chem. A*, 2019, **7**, 1556–1563.
185 Y. Fu, X. Zhu, L. Huang, X. Zhang, F. Zhang and W. Zhu, *Appl. Catal., B*, 2018, **239**, 46–51.
186 J.-L. Wang, C. Wang, K. E. deKrafft and W. Lin, *ACS Catal.*, 2012, **2**, 417–424.
187 Z. J. Wang, K. Garth, S. Ghasimi, K. Landfester and K. A. I. Zhang, *ChemSusChem*, 2015, **8**, 3459–3464.
188 Z. J. Wang, S. Ghasimi, K. Landfester and K. A. I. Zhang, *Adv. Mater.*, 2015, **27**, 6265–6270.
189 C. Su, R. Tandiana, B. Tian, A. Sengupta, W. Tang, J. Su and K. P. Loh, *ACS Catal.*, 2016, **6**, 3594–3599.
190 V. R. Battula, H. Singh, S. Kumar, I. Bala, S. K. Pal and K. Kailasam, *ACS Catal.*, 2018, **8**, 6751–6759.
191 C. Yang, Q. Jin, H. Zhang, J. Liao, J. Zhu, B. Yu and J. Deng, *Green Chem.*, 2009, **11**, 1401–1405.
192 R. D. Chakravarthy, V. Ramkumar and D. K. Chand, *Green Chem.*, 2014, **16**, 2190–2196.
193 B. Zhang, J. Li, B. Zhang, R. Chong, R. Li, B. Yuan, S.-M. Lu and C. Li, *J. Catal.*, 2015, **332**, 95–100.
194 Z. J. Wang, S. Ghasimi, K. Landfester and K. A. I. Zhang, *Chem. Commun.*, 2014, **50**, 8177–8180.
195 M. Liras, M. Iglesias and F. L. Sánchez, *Macromolecules*, 2016, **49**, 1666–1673.
196 J. Luo, X. Zhang and J. Zhang, *ACS Catal.*, 2015, **5**, 2250–2254.
197 P.-F. Wei, M.-Z. Qi, Z.-P. Wang, S.-Y. Ding, W. Yu, Q. Liu, L.-K. Wang, H.-Z. Wang, W.-K. An and W. Wang, *J. Am. Chem. Soc.*, 2018, **140**, 4623–4631.
198 J.-X. Jiang, Y. Li, X. Wu, J. Xiao, D. J. Adams and A. I. Cooper, *Macromolecules*, 2013, **46**, 8779–8783.
199 Y. Zhi, Z. Li, X. Feng, H. Xia, Y. Zhang, Z. Shi, Y. Mu and X. Liu, *J. Mater. Chem. A*, 2017, **5**, 22933–22938.
200 Y. Zhi, S. Ma, H. Xia, Y. Zhang, Z. Shi, Y. Mu and X. Liu, *Appl. Catal., B*, 2019, **244**, 36–44.
201 J. Luo, X. Zhang and J. Zhang, *ACS Catal.*, 2015, **5**, 2250–2254.
202 Z. Lia, Y. Zhi, P. Shao, H. Xia, G. Li, X. Feng and X. Chen, *Appl. Catal., B*, 2019, **245**, 334–342.

203 V. Polshettiwar, A. Decottignies, C. Len and A. Fihri, *ChemSusChem*, 2010, **3**, 502–522.
204 I. P. Beletskaya, F. Alonso and V. Tyurin, *Coord. Chem. Rev.*, 2019, **385**, 137–173.
205 Q. Xiao, S. Sarina, A. Bo, J. Jia, H. Liu, D. P. Arnold, Y. Huang, H. Wu and H. Zhu, *ACS Catal.*, 2014, **4**, 1725–1734.
206 F. Wang, C. Li, H. Chen, R. Jiang, L.-D. Sun, Q. Li, J. Wang, J. C. Yu and C.-H. Yan, *J. Am. Chem. Soc.*, 2013, **135**, 5588–5601.
207 Z. J. Wang, S. Ghasimi, K. Landfester and K. A. I. Zhang, *Chem. Mater.*, 2015, **27**, 1921–1924.
208 S. Ghasimi, S. A. Bretschneider, W. Huang, K. Landfester and K. A. I. Zhang, *Adv. Sci.*, 2017, **4**, 1700101.
209 C. Ayed, L. C. da Silva, D. Wang and K. A. I. Zhang, *J. Mater. Chem. A*, 2018, **6**, 22145–22151.
210 W. Zhang, J. Tang, W. Yu, Q. Huang, Y. Fu, G. Kuang, C. Pan and G. Yu, *ACS Catal.*, 2018, **8**, 8084–8091.
211 T. Robinson, G. McMullan, R. Marchant and P. Nigam, *Bioresour. Technol.*, 2001, **77**, 247–255.
212 I. K. Konstantinou and T. A. Albanis, *Appl. Catal., B*, 2004, **49**, 1–14.
213 X. Liu, J. Iocozzia, Y. Wang, X. Cui, Y. Chen, S. Zhao, Z. Li and Z. Lin, *Energy Environ. Sci.*, 2017, **10**, 402–434.
214 S. Ghosh, N. A. Kouamé, L. Ramos, S. Remita, A. Dazzi, A. Deniset-Besseau, P. Beaunier, F. Goubard, P.-H. Aubert and H. Remita, *Nat. Mater.*, 2015, **14**, 505.
215 S. Ghosh, N. A. Kouame, S. Remita, L. Ramos, F. Goubard, P.-H. Aubert, A. Dazzi, A. Deniset-Besseau and H. Remita, *Sci. Rep.*, 2015, **5**, 18002.
216 S. Ghasimi, S. Prescher, Z. J. Wang, K. Landfester, J. Yuan and K. A. I. Zhang, *Angew. Chem., Int. Ed.*, 2015, **54**, 14549–14553.
217 J. Wang, H. Yang, L. Jiang, S. Liu, Z. Hao, J. Cheng and G. Ouyang, *Catal. Sci. Technol.*, 2018, **8**, 5024–5033.
218 B. Wang, Z. Xie, Y. Li, Z. Yang and L. Chen, *Macromolecules*, 2018, **51**, 3443–3449.
219 Q. Huang, L. Guo, N. Wang, X. Zhu, S. Jin and B. Tan, *ACS Appl. Mater. Interfaces*, 2019, **11**, 15861–15868.
220 B. C. Ma, S. Ghasimi, K. Landfester, F. Vilela and K. A. Zhang, *J. Mater. Chem. A*, 2015, **3**, 16064–16071.
221 B. P. Biswal, H. A. Vignolo-González, T. Banerjee, L. Grunenberg, G. Savasci, K. Gottschling, J. Nuss, C. Ochsenfeld and B. V. Lotsch, *J. Am. Chem. Soc.*, 2019, **141**, 11082–11092.
222 Y. Bai, L. Wilbraham, B. J. Slater, M. A. Zwijnenburg, R. S. Sprick and A. I. Cooper, *J. Am. Chem. Soc.*, 2019, **141**, 9063–9071.

